

Nutrient and carbon export from a tidewater glacier to the coastal ocean in the Canadian Arctic
Archipelago

By

Patrick Lodge Williams

A thesis submitted in partial fulfillment of the requirements for the degree of
Master of Science

Department of Earth and Atmospheric Sciences

University of Alberta

© Patrick Lodge Williams, 2021

Abstract

As glaciers melt, a range of on-, in-, and under-glacier processes modify and export freshwater and sediments to the ocean. This glacial runoff may influence biological productivity in coastal ecosystems by supplying essential nutrients and labile carbon. Previous studies of glacial meltwater export to the ocean have primarily been conducted on rivers draining land-terminating glaciers, or in fjords with large tidewater glaciers. These studies speculate about downstream effects (river studies) or upstream causes (fjord studies) of differing carbon and nutrient availability and biological productivity, but do not measure them. Here, we conduct the first ice-to-ocean study at a marine-terminating glacier in the Canadian Arctic Archipelago (CAA). We characterize the nutrient and carbon content of ice and meltwater collected on the glacier surface, at its margins, and in the near-shore coastal ocean, all within 1 to 25-km of the glacier terminus. Results demonstrate that while meltwater from a shallow tidewater glacier did not directly increase downstream carbon and nutrient concentrations, it can induce upwelling of deeper nutrient-rich marine water. Also, although carbon concentrations in meltwater were low, results show that this carbon is potentially more bioavailable than marine carbon. Glacially-mediated delivery of labile carbon and upwelling of nutrient-rich water occurs in summer, when surface waters are nutrient-limited. Collectively, these processes could benefit surface marine plankton, potentially stimulating production at the base of the food web. Shallow tidewater glaciers are commonly retreating in Arctic regions like the CAA and Svalbard, and understanding how increased meltwater output from these systems impacts marine ecosystems is critical.

Preface

I was responsible for designing this research project, field season planning, running the sample analyses, and all data analysis. Maya Bhatia, Erin Bertrand, and David Burgess collected summer glacial and marine samples and retrieved time-lapse camera imagery. Stephanie Waterman processed the CTD data into individual profiles. David Burgess provided all historic mass-balance data. David Burgess, Stephanie Waterman, Megan Roberts, Erin Bertrand, and Maya Bhatia provided manuscript edits to chapter two. No part of this thesis has been previously published.

This thesis is divided into three chapters, beginning with an introduction, followed by a research chapter in manuscript form, and finally a concluding chapter. The first chapter introduces the overall context, relevance, and significance of my research and the overarching goals of this thesis. Chapter two, titled “Nutrient and carbon export from a tidewater glacier to the coastal ocean in the Canadian Arctic Archipelago,” is co-authored by David Burgess, Stephanie Waterman, Megan Roberts, Erin Bertrand, and Maya Bhatia. The manuscript is in preparation for submission to the *Journal of Geophysical Research: Biogeosciences*. The third chapter summarizes the research findings, provides an analysis of potential limitations, and finally, an explanation of ongoing work and future analyses.

Acknowledgments

To me, scientific inquiry is about learning to stand on the shoulders of giants. My legs are wobbly and I owe so much to so many. Thank you, Maya. Your patience, guidance, and support will be what I remember most from these last few years. My time working with you has taught me to be a better scientist and a better person. The opportunities and adventures that have come from this thesis are all thanks to you. I am, and will always be, grateful. Dave, your wisdom, humor, and stories in the field are an inspiration. Your help has been instrumental at every step of this project, from planning field seasons to interpreting climate models. I watched you reassemble a weather station in 50 km winds with blowing snow at -40°C . There was a pair of long-johns hanging like a scarecrow from a mass-balance pole behind you – and you weren't wearing gloves because “you couldn't feel what you were doing” with them on. You have taught me to stay outside and stay frosty. Erin, you have helped me maintain perspective throughout this thing. Sitting around your table in Halifax seems like ages ago, but your support has kept this thing on the rails. From field work to figures, your advice has been instrumental. Stephanie, your help in finding structure in both my data and my writing has made me a better scientist. R, Matlab, and topic sentences; I'd like to think I'm a little better at all three thanks to you. Seth, I asked you once how to survive a thru-hike and you told me to “keep searching for the small things and stay curious.” Your love and respect for learning is the standard to which I hold myself.

To everyone who put up with me in the field and lab. Megan, I have never been so sleep-deprived, or enjoyed my time more, than when we were chilling in the Arctic on an Icebreaker at 3:00 am throwing buckets. We ate ice cream on toast together, and anyone who will do that with you must be one of the good ones! Your joy and music have been an inspiration. Ashley, you

taught me how to function in the Arctic. We ate frozen sardines and jalapeños together in the middle of an ice cap at -40°C . If that doesn't summarize this whole experience, I don't know what does. Claire, your patience and creativity were what kept our gang together. You made a protractor out of a trash can lid and some twine so we could map the structure of a subglacial channel – one of the most scientifically badass stories I can tell. Brad, you are who I aspire to be in the field. Calm, cool, and totally prepared. Also, you have revolutionized my oatmeal game and I cannot begin explain how important that is. Maria, it's thanks to you that I was able to function in lab in the first place. Putting together Go-Flos at 10 pm the Thursday before shipping field gear up to Resolute was the first and only time I've ever broken a sweat while playing with children's toys. Your laughter and love of poultry always made work feel like play.

Thanks to all the sources of funding and scientific collaborators that helped with into this project. Funds from UANRA, University of Alberta Graduate Teaching Assistantships, New Frontiers in Research Fund: Exploration grant (to Erin Bertrand, Stephanie Waterman, and Maya Bhatia), Polar Continental Shelf Project grant (to Maya Bhatia), Campus Alberta Innovates Program research chair (to Maya Bhatia), NSERC Ship Time grant (to Jochen Halfar and Paul Myers), and the University of Alberta Start-up grant (to Maya Bhatia), have been instrumental in making this thesis a reality. This work could not have been completed without the help of Suzanne and her lab, the CERC Ocean Laboratory (Dalhousie University), Ming and the Biological Analytical Services Laboratory (University of Alberta). And a huge thanks to Brice for providing the RACMO2.3 data. Vince and Martin, thank for your time, patience, guidance, and reading recommendations! You two have brought rigor and perspective to this project and I am a better scientist for it.

To my dearest darlinest momsie and popsicle: this thesis is going on the fridge. Make some space next to the shellacked herring and banana slug. You two instilled in me a love and respect for the teachers in my life and the right to vote. Thank you, for all things bright and beautiful. Katherine Anna. Bro. You inspire me to be better. You walk through this world with an understanding heart and help me to laugh at all the poop jokes. Stay happy, stay angry, and do it for the children. Timbo, your words help me to remember that in a discipline that focuses on data, it's people who matter. Thank you for the nuggets of wisdom and Wikipedia holes. May your tales be tall, and the truth be even taller. Abby, I cannot wait to cook a meal in the same kitchen as you. I tried to find a good quote, but I got nothing for ya, head back to camp.

Table of Contents

<i>Abstract</i>	<i>ii</i>
<i>Preface</i>	<i>iii</i>
<i>Acknowledgments</i>	<i>iv</i>
<i>Table of Contents</i>	<i>vii</i>
<i>List of Tables</i>	<i>viii</i>
<i>List of Figures</i>	<i>ix</i>
<i>Plain Language Summary</i>	<i>x</i>
<i>Chapter 1: Introduction</i>	<i>1</i>
1.1 Climate change in the Arctic.....	1
1.2. Conceptual models of glaciers and mechanisms of near-shore effects.....	2
1.3. Jones Sound, Grise Fiord, and tidewater glaciers.....	4
1.4 Purpose and objectives.....	5
1.5. Rationale and significance.....	7
<i>Chapter 2: Nutrient and carbon export from a tidewater glacier to the coastal ocean in the Canadian Arctic Archipelago</i>	<i>10</i>
1. Introduction.....	10
2. Materials and Methods.....	15
2.1. Site Description.....	15
2.2. Field instruments and sampling.....	18
2.3. Laboratory analyses.....	22
2.4. Data processing and analyses.....	24
2.5 Glacier surface mass balance modeling.....	27
3. Results.....	29
3.1. Meltwater export.....	29
3.2. Meltwater nutrient delivery.....	31
3.3. Meltwater carbon delivery.....	33
3.4. Glacial meltwater in the near-shore marine environment.....	36
3.5. Meltwater impacts on the marine environment.....	42
4. Discussion.....	46
4.1. Plume dynamics in the near-shore environment.....	46
4.2. Nutrient and carbon export in glacial meltwater runoff to the surface ocean.....	48
4.3. Impact of the submarine discharge plume on the surface ocean.....	52
4.4. Glacier effects on primary productivity in front of a shallow tidewater glacier.....	54
5. Conclusions.....	56
<i>Chapter 2: Supplemental</i>	<i>59</i>
<i>Chapter 3: Conclusions</i>	<i>66</i>
1. Research Conclusions.....	66
2. Ongoing analyses.....	66
3. Limitations and future research.....	68
<i>Works Cited</i>	<i>72</i>

List of Tables

<i>Chapter 2: Nutrient and carbon export from a tidewater glacier to the coastal ocean in the Canadian Arctic Archipelago</i>	10
Table 2.1. Glacial freshwater and marine seawater values.....	33
Table 2.2. A summary of the 5 PARAFAC components.	35
<i>Chapter 2: Supplemental</i>	59
Table S2.1. Summary of samples collected and presented in this study.	64
<i>Chapter 3: Conclusions</i>	66
Table 3.1. Summary of characteristics of tidewater glaciers studied in the larger Jones Sound study. .	70

List of Figures

<i>Chapter 1: Introduction</i>	1
Figure 1.1. Schematic of possible upwelling scenarios for marine-terminating glacier systems. Adapted from Hopwood et al. 2018.....	8
Figure 1.2. Map of study area in Jones Sound.....	9
<i>Chapter 2: Nutrient and carbon export from a tidewater glacier to the coastal ocean in the Canadian Arctic Archipelago</i>	10
Figure 2.1. Map of study site.....	17
Figure 2.2. Sverdrup mass balance summary.....	31
Figure 2.3. Principal component analysis (PCA) of the five modeled PARAFAC components.....	36
Figure 2.4. Plots of $\delta^{18}\text{O}$, salinity, dissolved oxygen concentration, turbidity, nitrate concentration, and <i>Chl a</i> concentration along the “out” transect in Brae Bay.....	40
Figure 2.5. Plots of $\delta^{18}\text{O}$, salinity, dissolved oxygen concentration, turbidity, nitrate concentration, and <i>Chl a</i> concentration along the “near” and “distal” transects in Brae Bay.....	41
Figure 2.6. Boxplot of glacial melt fractions for all samples.....	42
Figure 2.7. Apparent oxygen utilization (AOU) versus nitrate, phosphate, silicate, and turbidity of marine water in Sverdrup Bay.....	44
<i>Chapter 2: Supplemental</i>	59
Figure S2.1. Summary of Sverdrup Glacier ice elevation and thickness.....	59
Figure S2.2. Sverdrup surface mass balance validation.....	60
Figure S2.3. Time-lapse camera image summary.....	61
Figure S2.4. $\delta^{18}\text{O}$ versus salinity.....	62
Figure S2.5. Box plots of marine nutrient ratios.....	63
<i>Chapter 3: Conclusions</i>	66
Figure 3.1. Comparisons of surface ocean waters at tidewater glaciers in the CAA.....	71

Plain Language Summary

As glaciers melt, nutrients and carbon contained in runoff may impact recipient marine ecosystems. The last study to explore the relationship between tidewater glaciers and nutrient availability in the Canadian Arctic Archipelago (CAA) was in the 1970s. Here we measure nutrient and carbon concentrations in ice, glacial melt, and marine waters in front of a shallow tidewater glacier in the CAA. We find that nutrient and carbon concentrations in glacial melt are not high enough to augment downstream marine concentrations. However, the carbon in glacial melt appears more protein-like and may be more bioavailable than marine carbon. Additionally, with the release of submarine discharge at the terminal ice front, glacial meltwater entrains deeper nutrient-rich marine water and delivers nutrients to the surface as the meltwater plume rises. This upwelling is associated with the turbid meltwater plume and higher concentrations of Chlorophyll *a*. Upwelling of nutrients forced by a shallow tidewater glacier, common in the Canadian Arctic, could locally benefit surface marine plankton and stimulate production at the base of the food web.

Chapter 1: Introduction

1.1 Climate change in the Arctic

Arctic ice masses (glaciers, ice caps, and the Greenland ice sheet) are melting more rapidly as a result of human-induced climate change (Stocker et al., 2014). Increases in anthropogenic greenhouse gases coupled with positive feedback mechanisms are causing the cryosphere to warm nearly twice as fast as the global average (Cohen et al., 2019; Wendisch et al., 2017). The underlying mechanisms of change include changes in sea ice extent and heat fluxes between the ocean and atmosphere, atmospheric and oceanic heat exchange, water vapor concentration and radiation flux to the surface, and black carbon on snow and heightened black carbon aerosol concentrations (Serreze & Barry, 2011). Recent work suggests that the impact of changes in the Arctic are not confined to the north, but are also apparent at lower latitudes, via alteration of storm paths, formation of deep water in the North Atlantic, and energy propagation over the rest of the planet (Cohen et al., 2014; Muschitiello et al., 2019). In the Canadian Arctic Archipelago (CAA), this warming is even more pronounced, and in 2019 was deemed “effectively irreversible” by Environment and Climate Change Canada, with warming rates nearly three times the global average (Bush & Lemmen, 2019). The CAA is especially susceptible to rising air temperatures because, more so than in Greenland, melt is heavily influenced by ambient air temperature, rather than warming ocean temperatures (Cook et al., 2019). Since it requires less time and energy to warm the atmosphere than the ocean, ice masses in the CAA are likely to respond faster to warming. This will make the CAA region and its residents subject to widespread and potentially unexpected environmental changes in the near future.

Ice masses in the CAA represent almost one-third of the global volume of land ice outside Greenland and Antarctica, with melt from this region, contributing ~92 Gt of freshwater annually to high-latitude oceans (Gardner et al., 2011). Much of this melt is routed through glaciers which terminate in the ocean (tidewater glaciers). Studies in other Arctic regions, such as Greenland, Alaska, and Svalbard, suggest that when this glacial runoff enters the coastal ocean, it can affect marine nutrient and carbon supply (Halbach et al., 2019; Hood et al., 2009; Wadham et al., 2016), coastal circulation (Straneo & Cenedese, 2015), and biological productivity (Juul-Pedersen et al., 2015; Meire et al., 2017; Meire et al., 2015). Nutrients and carbon entrained in glacial melt can be exported to the ocean, where they are used by primary autotrophs (nutrients) and heterotrophs (carbon). This influx of glacial melt occurs in the summer when marine production may be nutrient-limited following the drawdown of nutrients during the spring bloom (Tremblay et al., 2015). Therefore, nutrients and carbon in meltwater draining from ice masses in the CAA may stimulate recipient marine ecosystems that would otherwise be nutrient limited and less productive at a critical time of year.

1.2. Conceptual models of glaciers and mechanisms of near-shore effects

Understanding how glacier melt impacts marine ecosystem function at the base of the marine food web is essential to predicting how northern regions will be affected as Arctic ice masses melt. While both tidewater and land-terminating glaciers deliver meltwater downstream, previous studies in Greenland and Antarctica have found that runoff from land-terminating glaciers are associated with decreased coastal productivity whereas fjords with tidewater glaciers generally have elevated productivity (Arrigo et al., 2017; Carroll et al., 2016; Meire et al., 2017). Depending on the geometry of the glacier in question, exported meltwater enters the ocean via different

mechanisms. Four theoretical scenarios have been proposed by Hopwood et al. (2018) to explain how glacial melt enters the marine environment and impacts nutrient availability and biological productivity (Figure 1.1). In a land-terminating glacier (Figure 1.1d), meltwater streams deliver turbid, low density meltwater that forms a freshwater cap on the ocean surface (Chu et al., 2012; Ohashi et al., 2016). This input therefore impedes light penetration while also stratifying coastal waters and limiting vertical macronutrient supply from depth (Bergeron & Tremblay, 2014; Randelhoff et al., 2020a; Randelhoff et al., 2020b). Conversely, in deep tidewater glacier systems (Figure 1.1a), where the ice front terminates directly in the ocean, meltwater is released at depth as submarine discharge hundreds of meters below the surface. After release, the low-density fresh water rises along the calving front in a turbid plume (Mankoff et al., 2016). As it rises, this plume can entrain nutrient-rich deep water and transport it to the ocean surface (Cape et al., 2018; Hopwood et al., 2018; Kanna et al., 2018). At very deep discharge depths (>700 mbsl), however, the rising plume becomes neutrally buoyant below the photic zone, and photosynthetic organisms are unable to use the upwelled nutrients. Thus, at very deep tidewater glaciers, productivity will not be immediately enhanced, regardless of the volume of melt exported. In contrast, at tidewater glaciers with optimum discharge depths ($\sim 580 \pm 200$ mbsl), discharge also upwells and entrains nutrient-rich deep water, but the plume buoyantly equilibrates in the photic zone, delivering plume and deep water to the surface. If there are sufficient limiting nutrients (e.g., nitrate, phosphate, silicate, iron) or labile carbon in this deep water and/or glacial meltwater, surface productivity could increase. Finally, at shallow tidewater glaciers (Figure 1.1c), Hopwood et al. (2018) propose that discharge exits at depths too shallow to entrain nutrient-rich deep water. Using an idealized model that incorporated fjord geometry, hydrology, wind, tides, and phytoplankton growth, Oliver et al. (2020) also found that meltwater-driven nutrient export increased with larger subglacial

discharge rates and deeper grounding lines. Both of these features are likely to change with continued melting of ice in the Arctic.

Theoretical models (Hopwood et al., 2018; Oliver et al., 2020) predict that as glaciers melt and discharge depths shoal due to inland glacier retreat, and depending on bedrock geometries, delivery of essential nutrients to the near-shore environment during nutrient-limited summers could change. However, these models are based on data gathered in Greenland, where the average tidewater glacier discharge depths are deep – at ~280 m depth (Morlighem et al., 2017). Thus, it is challenging to extend these models to other Arctic regions (e.g., CAA, Svalbard) where glaciers are shallower. For example, this average discharge depth in Greenland is approximately 50-180 m deeper than it is at tidewater glaciers in the CAA (Van Wychen et al., 2014; Van Wychen et al., 2015). Indeed, across the CAA, only eight glaciers have grounding lines deeper than 300 m (Van Wychen et al., 2015). There are over 300 tidewater glaciers in the CAA (Cook et al., 2019), and the annual meltwater discharge delivered by these ice masses to the North Atlantic and Arctic oceans represents the largest contribution of freshwater from melting ice outside of the Greenland and Antarctic ice sheets (Box et al., 2018). Yet, despite this large flux, little is known about the effects of shrinking glaciers in the CAA on regional and coastal hydrography and biogeochemistry. Nor is it clear whether existing models that purport to explain how glacial melt impacts the coastal ocean apply to the shallower glaciers typical of the CAA.

1.3. Jones Sound, Grise Fiord, and tidewater glaciers

Though work exploring the impacts of glacial export on recipient marine environments is ongoing in other parts of the Arctic (e.g. Greenland, Svalbard) the most recent study on this topic in the CAA was conducted in Jones Sound (Nunavut) in the 1970s (Apollonio, 1973). This work

compared macro-nutrient concentrations in glacierized and non-glacierized fjords, implicating glacial activity in providing limiting macronutrients (nitrate, silicate) to local phytoplankton production. However, today, despite rapid acceleration of glacial melt in the CAA, there is a nearly a 50-year gap in our knowledge of how glaciers impact nutrient distribution, and thus primary production, in Jones Sound, or any CAA coastal waters. Recent work in glacierized regions in Greenland and Alaska has also shown that glaciers might export labile carbon to coastal ecosystems, fueling marine secondary (microbial heterotrophic) production in these regions. Jones Sound is a marine waterway surrounded by glaciers draining large ice fields and caps on Ellesmere and Devon Islands, and is home to the community of Grise Fiord (Ajuittuq).

Jones Sound is also a major oceanographic waterway through the CAA, contributing ~20% of the outflow from the CAA to the Labrador Sea (Melling et al., 2008; Zhang et al., 2016). Thus, if Jones Sound waters are heavily influenced by glacial melt, these impacts may extend beyond the sound itself to the broader North Atlantic. Traditional knowledge from residents of Grise Fiord suggests that the termini of glaciers in Jones Sound are highly productive, attracting marine mammals, and serving as the hunting grounds for its citizens. Hunting in this region provides a valued supply of country food, and is an important part of Inuit lifestyles. Understanding how increased glacial melt impacts nutrient and carbon availability, and by extension productivity at the base of the food web in this region, is critical to indigenous coastal communities, like Grise Fiord, across the CAA.

1.4 Purpose and objectives

This thesis builds on the initial work conducted by Apollonio (1973), focusing on a single shallow tidewater glacier (Sverdrup Glacier, Devon Island Ice Cap) draining into Jones Sound.

This project represents a first step towards a holistic understanding of how glacial meltwater discharge affects marine ecosystem productivity and health in the CAA. This thesis is also part of a larger study that explores the nutrient dynamics associated with multiple tidewater glaciers in Jones Sound that are of varying size and at different stages of retreat from the ocean (Figure 1.2). Chapter three uses selected data from this spatial study to provide additional context for data presented in this thesis.

To better understand and model glacially-mediated changes to the marine environment, we must first establish a baseline for quantifying the impact of CAA tidewater glaciers on biogeochemical cycles. Chapter two of this thesis focuses on the unresolved but potentially important role that glacial meltwater plays in downstream marine ecosystems by delivering nutrients and carbon to the ocean surface in the CAA. The goal of this study is to establish whether meltwater draining from a shallow tidewater glacier in the CAA can deliver nutrients and carbon to downstream environments as has been observed in other Arctic glacierized regions. I measure these chemical constituents in the glacier meltwater draining Sverdrup glacier, and then track the propagation of the meltwater discharge plume in the coastal ocean. My goals are to: 1) determine if the glacial meltwater itself is directly providing macronutrients to the coastal ocean; 2) determine if discharge from a shallow tidewater glacier can induce upwelling and entrain deep water nutrients to the ocean surface and 3) determine the degree to which primary producers are impacted by glacial discharge during the summer melt season. This work generates knowledge that can be used by the residents of Grise Fiord and other coastal communities to assess and plan for future ocean and ecosystem changes in Jones Sound and the broader CAA.

1.5. Rationale and significance

Given the sensitivity of CAA tidewater glaciers to climate change and the sweeping environmental changes already occurring as a result of a warming atmosphere, the CAA is a critically understudied region with respect to the broader impact of melting ice masses on recipient waters. To date, no single study has characterized the physical, chemical, and biological nature of glacially-derived submarine discharge or its transport and dispersal in the nearshore waters of the CAA. Northern oceans are highly productive, with both communities and industries (e.g. fisheries and tourism) relying on the continued good health of these high-latitude ecosystems. This thesis provides baseline data critical to resolving the relationship between melting glaciers and northern marine ecosystem productivity, function, and health. Results from this study provide new insight into glacier-ocean interactions and their relationship to nutrient and carbon availability in the CAA.

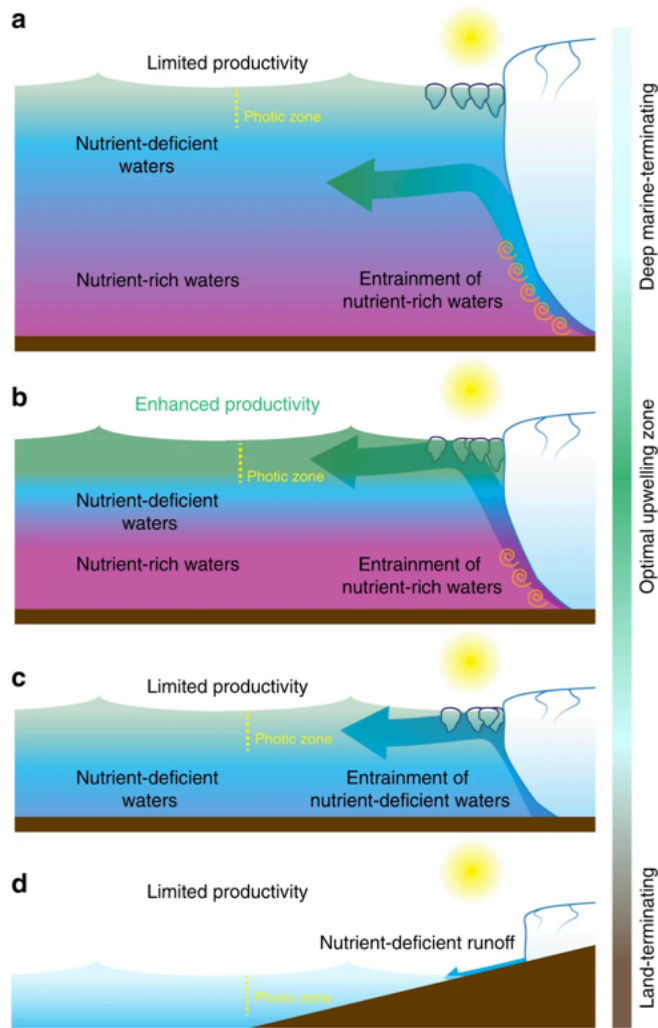


Figure 1.1. Schematic of possible upwelling scenarios for marine-terminating glacier systems. Adapted from Hopwood et al. 2018.

(a) Deeply grounded glaciers result in plumes that lose buoyancy through entrainment and equilibrate below the photic zone. (b) Glaciers grounded within the optimum zone for nutrient upwelling facilitate equilibration of a macronutrient-rich plume in the photic zone. (c) Plumes emerging from shallow glaciers equilibrate in the photic zone; however, they are unable to entrain deep, nutrient-rich seawater. (d) Runoff from land-terminating glaciers contain insufficient nutrients to drive enhanced productivity.

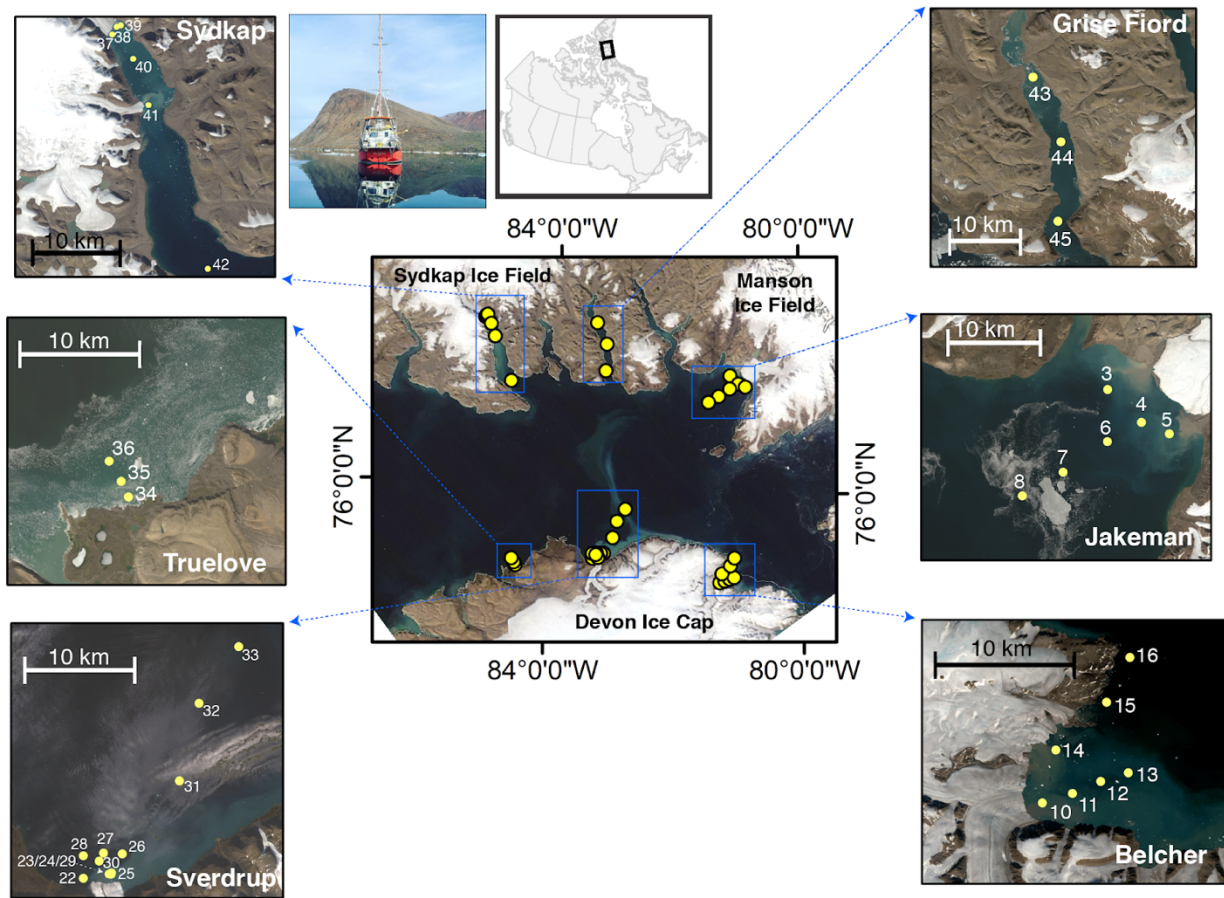


Figure 1.2. Map of study area in Jones Sound

Map of the broader study area in Jones Sound (NU) in the Canadian Arctic Archipelago using a MODIS image of the region from August 15, 2019. Blue boxes highlight six primary study sites, consisting of four tidewater glacier sites (Belcher, Sydkap, Sverdrup, and Jakeman glaciers) and two sites without glaciers (Truelove Lowland and Grise Fiord). Insets (using Landsat imagery from July and August 2019) show enlarged geographical areas and the sailboat S/Y Vagabond from which shipboard operations were conducted. Images courtesy of D. Burgess.

Chapter 2: Nutrient and carbon export from a tidewater glacier to the coastal ocean in the Canadian Arctic Archipelago

1. Introduction

Polar ice caps and glaciers in the Canadian Arctic Archipelago (CAA), Greenland and Antarctica are melting six times faster than they were 30 years ago in response to climate change (Shepherd et al., 2020). Compared to the polar ice sheets, the CAA is populated by smaller ice caps, icefields, and glaciers, and in the future, these ice masses may be particularly susceptible to warming air temperatures (Cook et al., 2019). Similar to Greenland and Antarctica, many ice caps and icefields in the CAA are drained by glaciers that terminate in the ocean (tidewater glaciers). Recent studies show that glacial runoff into the coastal ocean can affect marine nutrient and carbon supply (Hawkings et al., 2015; Hood et al., 2009; Wadham et al., 2016), coastal circulation (Straneo & Cenedese, 2015), and biological productivity (Juul-Pedersen et al., 2015; Meire et al., 2017; Meire et al., 2015). Since most previous work investigating glacially-mediated nutrient delivery has been undertaken on large tidewater glaciers in Greenland, it is not clear whether the mechanisms by which large tidewater glaciers promote marine productivity apply to the smaller ice masses present in the CAA (Hopwood et al., 2018).

Traditional knowledge from northern communities document waters off glacier termini to be rich in wildlife (pers. comm. J. Qaapik, Grise Fiord Rangers). In 1938, “brown zones” in waters adjacent to glaciers around Disko Bay (Greenland) were identified as areas of upwelling that

supported large populations of coastal birds (e.g. Kittiwake) which fed on zooplankton in a freshened meltwater plume (Hartley & Dunbar, 1938). The ability of glaciers to erode and deliver rock-derived nutrients like silicate (SiO_4^{4-}) and phosphate (PO_4^{3-}), important to downstream phytoplankton communities, was also recognized early in the 20th century (Vibe, 1939). In the most recent study of glacially-derived nutrients in marine waters in the CAA, Apollonio (1973) found elevated concentrations of nitrate (NO_3^-) and silicate within a glacierized fjord when compared to a non-glacierized fjord before the spring thaw. Apollonio noted that these nutrients were critical to arctic phytoplankton and augmented by glacial activity.

One main mechanism by which glacial melt can deliver nutrients and carbon to downstream marine environments is via direct delivery of chemical constituents in meltwater. In early summer, glacial runoff consists predominantly of surface snow melt which delivers a source of atmospherically-deposited nitrate to the marine environment (Wolff, 2013). As the melt season progresses, the proportion of ice melt in glacial runoff increases (Nienow et al., 1998; Richards et al., 1996), which drains from the surface to the glacier bed via crevasses and moulins (Boon & Sharp, 2003; Das et al., 2008). At the bed, glacial meltwater can become chemically enriched in crustally-derived nutrients (e.g. silica, iron, and phosphorus) and carbon (Bhatia et al., 2013b; Hawkings et al., 2016; Hawkings et al., 2017; Hood et al., 2009) before discharging into the marine environment (Kanna et al., 2018). Numerous studies suggest that *in situ* microbial communities on the glacier surface or at the bed are capable of high rates of biogeochemical/physical weathering and cycling of organic carbon (Dubnick et al., 2017; Dubnick et al., 2020). *In situ* microbial nitrogen fixation at the glacier bed is a second important source of nitrate that may be delivered to marine waters (Boyd et al., 2011; Segawa et al., 2014; Telling et al., 2012; Wadham et al., 2016). These communities can further provide labile protein-like dissolved organic matter (DOM) to

downstream environments (Bhatia et al., 2010; Hood et al., 2009; Musilova et al., 2017). Over the course of the melt season, basal flow evolves from a slow and distributed system, dominated by snow-melt and basal ice-melt, to a fast and channelized one, dominated by ice-melt originating from the surface (Flowers, 2015; Gray, 2005; Hubbard et al., 1995). This evolution leads to shorter retention and rock-water interaction times at the bed, and consequently lower entrained nutrient and carbon concentrations/fluxes during peak melt (Brown, 2002; Sharp, 2005).

A second mechanism by which glacial melt can facilitate nutrient addition to coastal waters is indirectly, via promoting the delivery of nutrients in deep nutrient-rich marine waters to the near-surface by entrainment, upwelling, and mixing. At the terminus of tidewater glaciers, runoff exits sub-glacially, sometimes hundreds of meters below the ocean surface (Straneo & Cenedese, 2015). As the buoyant meltwater plume rises, it can entrain deep marine water containing elevated levels of macronutrients (nitrate, phosphate, silicate) and transport it to the surface. This entrainment of nutrient-rich deep water has been tied to locally high rates of primary production observed in glacial fjords in Greenland and Svalbard (Halbach et al., 2019; Kanna et al., 2018; Meire et al., 2017). Additionally, estuarine circulation in fjords fed by glaciers can also drive upwelling and play an important role in nutrient delivery to the ocean surface in areas influenced by freshwater (Etherington et al., 2007). The strong tidal currents and shallow sill (moraine) entrances associated with glacial fjords and bays can further enhance vertical mixing, which in turn can enhance the delivery of deep-water nutrients to the surface (Etherington et al., 2007).

In the ocean, directly- or indirectly-sourced glacially-derived nutrients may fuel primary autotrophic producers (phytoplankton) while labile carbon can feed microbial heterotrophs. Phytoplankton communities require a host of macro- (e.g. nitrogen, phosphorus, silica) and micro- (e.g. iron) nutrients to grow, but in the Arctic waters during the summer months, nitrogen (N) is

generally limiting following the spring bloom (Sorensen et al., 2017; Tremblay & Gagnon, 2009; Zhu et al., 2019). Since glacier meltwater delivery to the ocean occurs when NO_3^- concentrations in surface waters are near zero, coastal phytoplankton communities could be dependent on glacially-derived nutrients to sustain summer growth (Cape et al., 2018; Kanna et al., 2018; Meire et al., 2017). In tandem, microbial heterotrophs may use glacially-derived carbon, further stimulating higher trophic levels via the microbial loop (Azam & Malfatti, 2007). Previous studies have found marine DOM to be recalcitrant, characterized by high humic-like components, while glacial DOM tends to be more protein-like (bioavailable), suggesting that glacially-derived carbon may better support downstream heterotrophic productivity (Bhatia et al., 2013a; Hood et al., 2009; Musilova et al., 2017). The positive effects of glacial meltwater on the availability of nutrients and carbon, and ultimately on productivity, are not necessarily restricted to areas close to glacier termini, and they may extend further from shore to the continental shelf (Cape et al., 2018; Painter et al., 2014).

Most previous work studying how glaciers impact marine nutrient and carbon availability has been conducted either at land-terminating glaciers or in the ocean at large tidewater glaciers. While some studies that span the ice-to-ocean continuum do exist (Halbach et al., 2019; Kanna et al., 2018), there is a notable lack of research that considers the full ice-to-ocean system (Hopwood et al., 2018; Meire et al., 2017). The absence of concurrent measurements on the ice and in the ocean makes it challenging to determine whether enhanced nutrient concentrations observed in coastal waters near tidewater glaciers (Kanna et al., 2018; Meire et al., 2017) are controlled by direct delivery, deep water entrainment, or enhanced estuarine circulation. Additionally, the regional focus on glacier systems in Greenland to date has led to a bias in the modern literature towards large glaciers with deep submarine discharges draining into long fiords at depths ≥ 140

meters below sea level (Cape et al., 2018; Kanna et al., 2018; Meire et al., 2017). This bias may be problematic as according to these studies, the strength of meltwater-induced upwelling, and thus the rate of indirect nutrient delivery, is largely dependent on the depth at which submarine discharge enters the ocean and thus on the depth of the glacier grounding line (Hopwood et al., 2018). Numerical models, based on these Greenland studies and parameterized using deep outlet glacier systems (Hopwood et al., 2018; Oliver et al., 2020), propose a productivity continuum between tidewater and land-terminating glaciers. These models predict that as submarine discharge from tidewater glaciers becomes shallower, less nutrient-rich deep water is delivered to the surface, and productivity enhancements decline as a result (Hopwood et al., 2018). Further, these models indicate that if the glacier grounding line shoaled above a given threshold depth (280 ± 200 m depth in the numerical model studied by Hopwood et al.), indirect nutrient delivery becomes decoupled from the glacier meltwater flux, suggesting that deep and shallow tidewater glaciers may impact indirect nutrient delivery to shallow waters in different ways.

Very few measurements have been made at intermediate-depth (Meire et al., 2017) and shallow-outlet (Halbach et al., 2019) tidewater glaciers. However, across the Arctic, intermediate-depth and shallow-outlet tidewater glaciers are common. For example, in the Queen Elizabeth Islands (northern CAA), the grounding line depth of tidewater glaciers averages ~ 230 m depth (Van Wychen et al., 2014) while on Baffin and Bylot Islands (southern CAA) grounding lines are estimated to be ~ 100 m depth on average (Van Wychen et al., 2015). Similarly, in the Svalbard archipelago, the average grounding line depth is estimated to be ~ 100 m depth (Błaszczuk et al., 2009). These glacier systems are significantly shallower than typical tidewater glaciers in Greenland, where the average grounding line depth is ~ 280 m depth (Morlighem et al., 2017). Further, there is in situ evidence that shallow-outlet tidewater glaciers have the potential to

positivity impact productivity: in a recent study of tidewater glaciers with grounding lines of ≤ 70 m depth in Kongsfjorden, Svalbard, Halbach et al., (2019) reported the presence of glacially-induced upwelling of nutrients in the fjord. Considering this result and the prevalence of shallow-to-intermediate depth outlet tidewater glaciers across the Arctic, further observations of shallow-terminating tidewater glaciers are necessary to gain a more complete understanding of the impacts of melting glaciers on coastal biogeochemistry.

With the goal of determining how a shallow tidewater glacier impacts nutrient and carbon availability in the proximate ocean, we conducted an ice-to-ocean study at Sverdrup Glacier, Devon Island in the CAA. In contrast to many previous study sites, submarine discharge exits Sverdrup Glacier relatively close to the surface. Here, we present *in situ* observations along a full ice-to-ocean transect with observations extending from the glacier surface and margins upstream of the glacier terminus, through the turbid subglacial discharge plume in the coastal ocean, to more than 25 km out into open water (Jones Sound). Our study builds upon a very small number of studies that have incorporated both on-ice and marine data to date (Halbach et al., 2019; Kanna et al., 2018), and is the first in the CAA to document the biogeochemical influence of glacial melt routed through the marginal and subglacial environments from ice to ocean.

2. Materials and Methods

2.1. Site Description

2.1.1 Sverdrup Glacier

In 2019, spring (April 12 - May 12) and summer (July 22 - August 16) field sampling campaigns were undertaken on Sverdrup Glacier, a warm-based marine-terminating glacier located on the north coast of Devon Island, Nunavut Canada that drains ~ 805 km² (RGI

Consortium, 2017) of the northwest sector of Devon ice cap. The 25-km long warm-based glacier overrides Precambrian metamorphic rocks of the Cumberland batholith, comprised primarily of granulitic high-K to shoshonitic monzogranite and granodiorite, and small amounts of low- and medium-K granitoid rocks (St-Onge et al., 2009; Whalen et al., 2010). Sverdrup Glacier's north-south oriented valley is bordered by steep walls with an average height of 300 m above the glacier surface (Vöggtli, 1967). Surface mass balance and ice velocity measurements were first made on Sverdrup Glacier in the 1960s (Koerner, 1970; Koerner et al., 1961; World Glacier Monitoring, 2008), and six automatic weather stations (AWS) have been measuring air temperature and changes in height of the ice/snow surface within the Sverdrup glacier basin since 1999. The *in-situ* measurements of ice velocity have shown that glacier flow rates typically increases early in the melt season, an event first measured in 1961 (Cress & Wyness, 1961). This seasonal acceleration points to a well-connected englacial/subglacial hydrological system driven by inputs of supraglacial and ice-marginal meltwater draining to the glacier bed upstream from the terminus (Wyatt & Sharp, 2017).

Recent monitoring of Sverdrup glacier has shown larger annual melt volumes associated with changes in climate. As of 2005, the ablation (<1375 m elevation) and accumulation (≥ 1375 m elevation) zones show average ice thickness changes of -0.58 ± 0.25 Gt/y w.e. and -0.33 ± 0.17 Gt/y w.e. respectively. Between 2000-2004, the melt season on Devon Island lasted 42.1 ± 6.3 days (Wang et al., 2005), and from 2004-2010, the length of the summer melt season on Devon Island has increased by 3.4-8.8 days depending on elevation (larger increases at lower elevations) as a result of increased advection of warm air into the CAA (Gascon et al., 2017).

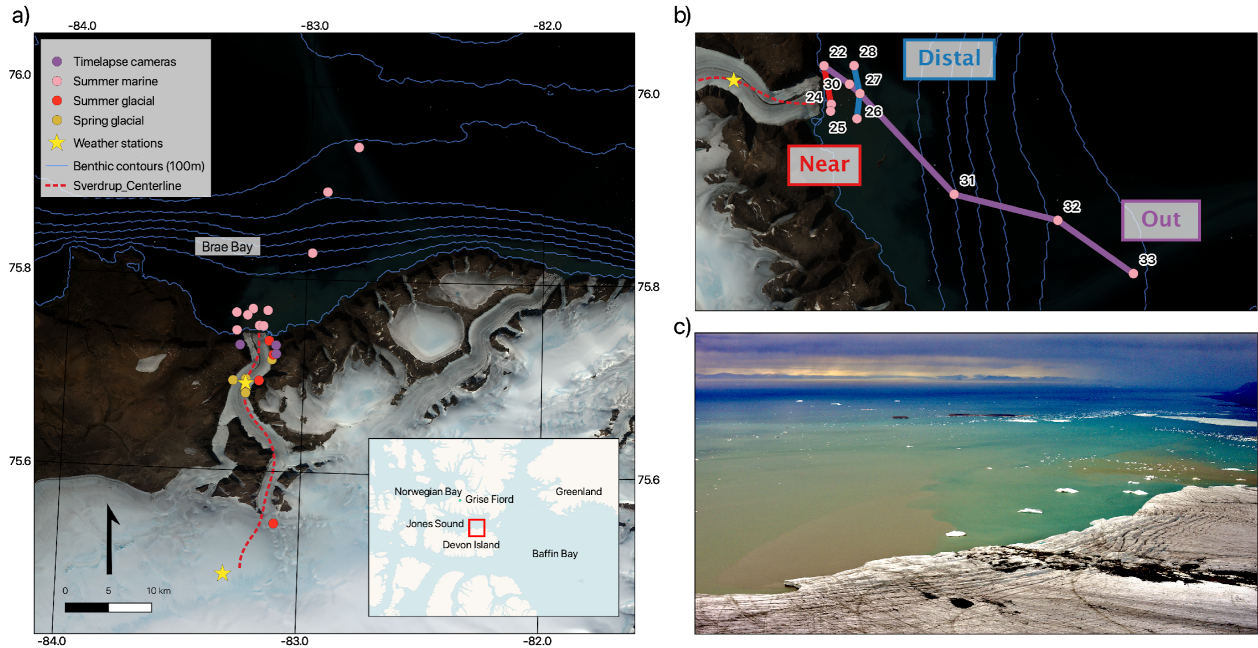


Figure 2.1. Map of study site.

(a) Map of Sverdrup Glacier (Devon Island, Nunavut) showing 2019 spring on-ice (orange) and summer (red) sample sites, summer marine stations (pink), time lapse camera locations (purple), weather stations (yellow stars), bathymetry (blue lines), and the 2012 IceBridge centerline (red dotted line). (b) Enlarged view of Brae Bay showing the three “near” (red), “distal” (blue), and “out” (purple) transects used in this study. (c) View of the terminus of Sverdrup Glacier on July 23, 2019 taken from the western terminus time-lapse camera (orange circle outlined in pink) showing the turbid freshwater plumes at the glacier front. Image brightness and contrast have been heightened for better plume visualization (see Methods).

2.1.2 Marine Setting

Meltwater from Sverdrup Glacier discharges into a protected inlet, Brae Bay, Jones Sound (Figure 2.1). The 5.12 km calving front is grounded on the seafloor (Dowdeswell et al., 2004) with an annual calving flux of 0.006 Gt/y (Van Wychen et al., 2020). Based on a single airborne radar sounding transect from the 2012 NASA Ice Bridge field program, (Paden et al., 2019), ice thickness within 1 km of the terminus is $\sim 20 \pm 10$ m (Sup. Figure 2.1). Unfortunately, the location of this centreline thickness measurement (Figure 2.1, red dotted line) does not coincide with that of the outflows of either of the submarine plumes observed in 2019. While much of the surface

meltwater runoff from Sverdrup Glacier is routed ice-marginally at higher elevations, historical field observations, as well as those made in 2019, reveal that the bulk of marginal meltwater enters the subglacial environment within 4 km of the glacier terminus (Keeler, 1964; Koerner et al., 1961). Due to the relatively low ice flow velocities on Sverdrup glacier (Cress & Wyness, 1961), fewer iceberg calving events have been observed here compared to other tidewater glaciers draining the ice cap (Cress & Wyness, 1961; Dowdeswell et al., 2004). This makes Sverdrup's terminus more readily accessible for oceanographic work than the termini of more active glaciers.

Once released into the marine environment, meltwater enters Jones Sound, a waterway between Devon Island and the southern end of Ellesmere Island. Water from the Arctic Ocean enters Jones Sound via Cardigan and Hellgate to the west and from Nares Strait to the east. Within Jones Sound, currents are cyclonic and the bulk of water exits the Sound into Baffin Bay and ultimately the North Atlantic (Barber & Huyer, 1977; Melling et al., 2008; Zhang et al., 2016). The bay in front of Sverdrup Glacier (Brae Bay) is hemmed by a series of submarine moraines extending ~9 km off-shore from Sverdrup's existing terminus; these moraines are located in shallow water, with some located less than 2 m below the surface (CHS Nautical Chart 7310, 2011).

2.2. Field instruments and sampling

2.2.1 *On-Ice Instrumentation and Sampling*

On-ice point measurements of surface mass balance were obtained from a network of 43 stakes drilled into the ice, and two automatic weather stations (AWS's) (Sup. Figure 2.1) in order to validate spatially continuous gridded model data across the Sverdrup glacier basin. The mass balance stake network spans the full elevational range from 100 to 1800 m a.s.l. including all

glaciological zones within the Sverdrup glacier basin. The upper AWS, i.e. DICS, used in this study is situated at 1300m a.s.l., near the long-term equilibrium line altitude, while the lower SVD station at 400 m a.s.l. is located in the ablation zone where the glacier surface thins by ~ 1 m annually due to summer melting. Air temperature and change in ice/snow surface height data from these AWSs (Figure 2.2) provide high temporal (hourly) resolution for tracking the evolution of the melt season; the latter are used to further assess bias in surface height modelling (see Section 3.1).

Time-lapse cameras were deployed at three different locations on the glacier in April 2019 (Figure 2.1) to capture the seasonal evolution of surface and marginal melt and to constrain characteristics of the freshwater plume that enters Jones Sound. These installations used Nikon D-3200 cameras fitted with Nikkor 28 mm lenses to capture high-quality JPEG images. Cameras were programmed to take an image every hour, provided there was enough light. The first photo was taken on April 28, 2019 and images were downloaded on August 9, 2019. 271 photos were taken by the time lapse cameras, but only images that were taken after the sea ice broke up and were minimally impacted by cloud / fog were used (13 images total).

Spring samples from different glacier “end-member” freshwater sources (basal ice, supraglacial snow / ice, and water stored at the base) were collected between April 23 and May 7, 2019. Bulk ice / snow / water samples were collected aseptically in trace metal clean ProPak® bags (Teledyne ISCO) using an ethanol-rinsed and flame-sterilized steel chisel and aluminum ice axe. Dissolved Organic Carbon (DOC) concentration and DOM fluorescence samples were collected in pre-combusted amber glass EPA vials with PTFE-lined septa. DOC samples were acidified with trace-metal grade concentrated HCl after collection to $\text{pH} \approx 2$. Samples were stored frozen and in the dark until analysed in the laboratory.

Summer 2019 freshwater melt samples from supraglacial and marginal runoff streams were collected between July 29 and August 15 and filtered in the field. Samples were collected in cleaned and sterilized 2 L Teflon bottles. Nutrient and oxygen isotope samples were filtered with sterile 60 mL plastic syringes, passed through a 0.22 μm polyethersulfone (PES) filter, and stored in HDPE scintillation vials. Oxygen isotope samples were stored in the dark at ambient temperature and nutrient samples were frozen within a few hours of collection. Samples for DOC, Total Dissolved Nitrogen (TDN), and DOM fluorescence were filtered with all-plastic polypropylene syringes (Norm-Jet), passed through a 0.22 μm PES filter, acidified to $\text{pH}\approx 2$ (DOC only) and stored in EPA vials as described above.

2.2.2 Marine Sampling

Ship-board work conducted from a polar sailboat (*S/Y Vagabond*) sampled the marine waters in front of Sverdrup Glacier from August 4-8, 2019 (Figure 2.1). Sensor-based hydrographic measurements, echo soundings, and bottle samples were taken at 12 marine stations, of which 10 spanned three individual transects (“near”, “distal”, and “out”) in front of the glacier terminus. Coordinates for all stations are provided in Sup. Table 2.1. Two lateral transects, one termed “near” (located ~ 0.8 km from the ice terminus, stations 22, 24, and 25) and the other “distal” (located ~ 2.5 km from the ice terminus, stations 26, 27, and 28), were sampled to gain insight into how glacial melt altered the near-shore marine environment in Brae Bay. The third transect (“out”, stations 22, 27, 30, 31, 32, and 33) followed the dispersion of a turbid plume from within 1 km of the ice terminus to >25 km out into Jones Sound in order to track the evolution in water column properties with increasing distance away from glacier terminus.

At each marine station, *in situ* measurements of electrical conductivity, temperature, pressure, dissolved oxygen, photosynthetically active radiation, Chlorophyll a (Chl a), and turbidity were made using a RBRmaestro3 profiler (hereafter CTD). The CTD was hung from a Dynema rope and at each station was allowed to equilibrate just below the surface. The CTD was lowered by a winch at a rate of less than 1 m/s and recorded measurements at a frequency of 8 Hz. All data presented here were collected during the downcast.

Marine bottle sampling was also conducted at each station. Sample depths were chosen using data collected during the CTD downcast and visualized in real-time with the Ruskin iOS and Android app (RBR Ltd. 2017). At each station, multiple sample depths were selected: a near-surface depth, the depth of the deep chlorophyll maximum (if present), and one or two deeper sample depths (in the range of 50-400 m depth).

Marine water samples were collected using 10 L Teflon-lined, trace-metal-clean Go-Flo bottles (General Oceanic) that had been soaked in 0.1% acid detergent (Citranox), rinsed 3x with MilliQ, cleaned with isopropanol, soaked in 0.2 M HCl for 12 hours, and rinsed 3x with MilliQ (Cutter & Bruland, 2012). Nutrient and oxygen isotope samples were collected directly from the Go-Flo bottles with silicon tubing and filtered and stored as described above for the summer freshwater samples, with nutrient samples immediately frozen after filtration. DOC, TDN, and DOM fluorescence samples were also collected from the Go-Flo bottles into 2 L Teflon bottles, and filtered, preserved and stored like the summer freshwater samples described above. Chl a samples were collected in 4 L polycarbonate bottles, and between 600-1600 mL was vacuum-filtered through a GF/F Whatman 47 mm filter in the dark, and then immediately frozen. All plasticware, glassware, and tubing was soaked overnight in a 10% HCL bath and washed 3x with MilliQ water. Glassware was then combusted at 560°C for ≥ 4 hours. All solvents used for cleaning

and sample analysis were trace-metal grade or better. In the field, plasticware and glassware were rinsed 3x with sample water prior to collection.

2.3. Laboratory analyses

Prior to analysis, all frozen on-ice freshwater samples were thawed in a glass beaker in the dark at 4 °C. Frozen marine samples were thawed in the dark at 4 °C in the original collection bottles. Samples for nutrients (nitrate, nitrite, ammonia, phosphate, silicate), oxygen isotopes, DOC, TDN, and DOM fluorescence properties were filtered through a glass vacuum apparatus with 0.22 µm Teflon (PTFE) Omnipore filters into scintillation vials.

On-ice freshwater nutrient samples (nitrite, nitrate, phosphate, silicate, and ammonia) were analyzed on a Lachat QuikChem 8500 series 2 flow injection analyzer at the Biological Analytical Services Laboratory (University of Alberta), via photometric detection for simultaneous measurement of nutrient concentrations. Samples and reagents were continuously pumped through the system, loaded onto one or more injection valves, and mixed in the QuikChem manifold under laminar flow conditions. Limits of detection (LODs) for nitrite+nitrate, nitrite, ammonia, phosphate, and silica were: 0.15, 0.15, 0.21, 0.06, and 0.71 µM respectively.

Marine nutrient samples (nitrite, nitrate, phosphate, silicate, and ammonia) were analyzed on a Skalar SAN++ Continuous Flow Nutrient Analyzer at the Canada Excellence Research Chairs Ocean Laboratory (Dalhousie University). Reagents and samples, segmented with air bubbles, were pumped through a manifold for mixing and heating before entering the flow cell. Nitrite, nitrate, phosphate, and silicate concentrations were detected colorimetrically with optical background correction, while ammonia concentrations were determined with a fluorometer. LODs

for nitrite, nitrate, ammonia, phosphate, silicate were: 0.3, 0.15, 0.01, 0.2, and 0.08 μM respectively.

DOC and TDN for both on-ice freshwater and marine samples were measured on a Shimadzu TOC-V (CPH) analyzer. DOC was quantified as non-purgeable organic carbon (NPOC) via high temperature combustion (680 °C) and TDN was measured with a total nitrogen module. A 6-point standard curve was used with $R^2 \geq 0.9986$ and $R^2 \geq 0.9994$ for DOC and TDN respectively. Standards were diluted from a 0.5 ppm stock solution for DOC (AccuSPEC, SCP Science) and from potassium nitrate for TDN (Sigma, KNO_3) analyses. Reference standards for deep seawater and low carbon water were obtained from the Consensus Reference Materials Project (Hansell Laboratory, University of Miami). MilliQ blanks and reference waters were analyzed routinely to monitor instrument drift, and remained within 5% of accepted values. The LOD was 2.5 μM for DOC and 3.33 μM for TDN. Procedural blanks using MilliQ water filtered through the plastic syringe and omnipore filters used in sample collection had DOC and TDN concentrations below the detection limit.

The fluorescent characteristics of DOM were analyzed with a Horiba Aqualog-3 spectrofluorometer equipped with a xenon lamp. Samples were brought to room temperature before analysis in a quartz glass cuvette with a 10 mm path length. Absorbance and excitation scans were measured in 5 nm intervals from 230-600 nm with an integration time of 10 s with 10 nm slits. Emission spectra were measured from 218-618 nm with an excitation offset of 18 nm. Ultrapure water in a dedicated cuvette (Mandel Scientific, SN-RM-H20) was used to validate the instrument. Excitation emission matrices (EEMs) were corrected with a MilliQ blank using the same settings.

Freshwater oxygen and deuterium isotopes were measured on a Picarro (L2140-i) at the University of Alberta while marine isotopes were measured on a Picarro (L2130-i) at Dalhousie University. A volume of one μL of water was injected, vaporized, and introduced into the analyzer and measurements of $\delta^{18}\text{O}$ and δD were obtained using cavity ring down spectrometry. Certified water standards (USGS-46 and USGS-48) were used to normalize raw isotope ratios to the Vienna Standard Mean Ocean Water-Standard Light Antarctic Precipitation (VSMOW-SLAP) scale. For both instruments, analytical error was $<0.5\text{‰}$ for δD and $<0.15\text{‰}$ for $\delta^{18}\text{O}$ (one standard deviation) based on routine analysis of an internal deionized water standard (QCDI 6-2).

Chl *a* was measured using a Turner Designs AquaFluor Handheld Fluorometer following EPA Method 445 (Arar & Collins, 1997). Whatman 47 mm GF/F filters were extracted in 10 mL of 90% acetone for 18-24 hours. A 5 mL aliquot of the supernatant was transferred to a glass cuvette and the fluorescence was measured. Samples were then acidified to 0.003 N using 0.1 N HCl and fluorescence was measured again to account for interference from non-photosynthetic phaeopigments. The fluorometer was calibrated using a pure Chl *a* standard (C5753, Sigma). The LOD for Chl *a* analysis was 0.024 $\mu\text{g/L}$ of seawater.

2.4. Data processing and analyses

2.4.1 Plume detection from time-lapse images

A k-means pixel classification was performed on a subset of the images from the time-lapse camera (13 images total) following Danielson and Sharp (2017) to detect the extent of the plume exiting Sverdrup's terminus. To minimize the effects of the sun's reflection, only images taken between 22:00 and 04:00 UTC were used. Land and sky were masked before pixel classification commenced. The k-means algorithm allowed for color-based plume detection at

Sverdrup's terminus in a variety of light conditions. The process followed four steps: 1) data cleaning, filtering, and color-correction; 2) k-means classification; 3) pixel area to relative area conversion; and 4) comparison of plume area over time. The k-means pixel classification was conducted in R following the algorithms described in (MacKay, 2003). Ten clusters were used in the analysis. While the clustering analysis detected the plume, the calculated color was not consistent across images and was therefore selected manually for each image. Converting pixel areas to relative areas was also done in R using a monophotogrammetric technique from Krimmel and Rasmussen (1986).

2.4.2 CTD data processing

Raw CTD data were processed using the Matlab *rsktools* toolbox distributed by RBR Ltd. Measured conductivity, temperature, and water pressure were used to derive salinity, depth, and seawater density according to the 2010 thermodynamic equation of seawater (McDougal & Barker, 2011). Salinity, depth, dissolved oxygen, PAR, Chl *a*, and turbidity vertical profiles were built by applying a low-pass filter to match sensor time constants using a three-sample running average, and channels were binned by pressure into 1-m intervals for further analysis. The euphotic zone depth, defined as the depth at which PAR=0.1% of the surface value (see Banse, 2004), was also calculated at each station using CTD measurements of PAR.

2.4.3 Optical properties of DOM

Parallel Factor Analysis (PARAFAC) is a statistical tool used to decompose trilinear data arrays to identify and quantify independent underlying signals or “components” (Bro, 1997). This technique can be applied to EEMs (excitation/emission matrices - a three-order array of sample

name, excitation wavelength, and emission wavelength) to break down complex spectra into generalized DOM components (Stedmon & Markager, 2005). While these components cannot be ascribed to specific organic species, they can be compared to previously described DOM fractions. The drEEM toolbox in Matlab (Murphy et al., 2013) was used to model five individual fluorescent components. Corrections for instrument spectral bias and inner filter effects were applied and Raman scatter was normalized using daily scans. EEMs were smoothed and normalized to unit variance. PARAFAC models were validated using split-half analysis (Murphy et al., 2013), making sure that each split dataset contained a mix of fresh and marine samples. Modeled components were compared to previous glacial studies (Dubnick et al., 2017; Fellman et al., 2010a; Fellman et al., 2010b; Hood et al., 2009; Pautler et al., 2012; Walker et al., 2009) and other published models in the OpenFluor database (Murphy et al., 2014). To summarize optical DOM composition across samples, fluorescent intensity of each component was summed and normalized. Principal component analysis (PCA), analysis of variance (ANOVA), and permutational multivariate analysis of variance (PERMANOVA) were subsequently performed in *R* using the *vegan* package.

2.4.4 Apparent oxygen utilization calculations

Apparent oxygen utilization (AOU) is the difference between measured dissolved O₂ and the theoretical equilibrium saturation concentration in water with the same physical and chemical properties. Differences between measured and theoretical dissolved O₂ concentrations are usually a result of biological activity: elevated primary production increases dissolved oxygen concentration, while respiration consumes oxygen and decreases dissolved oxygen concentration. Thus, AOU can be a measure of the sum of all biological activity a sample has undergone since its

last contact with the surface (Garcia et al., 2013). AOU was calculated using measured temperature, dissolved oxygen, and salinity as per Benson and Krause (1984) with the *LakeMetabolizer* toolbox in R.

2.4.5 Statistical analyses

All further statistical analyses were conducted in R using the *akima*, *candisc*, *caret*, *cowplot*, *ecodist*, *ggbiplot*, *ggisoband*, *interp*, *klaR*, *MASS*, *MBA*, *NISTunits*, *oce*, *ocedata*, *openair*, *gdal*, *RVAideMemoire*, and *zoo* packages.

2.5 Glacier surface mass balance modeling

Finally, in order to better constrain the meltwater inputs to the marine system we modelled the surface mass balance of the Sverdrup Glacier basin for the time period spanning our on-ice and marine observations. To do this, we estimate total meltwater runoff for the Sverdrup glacier basin (as defined by the Randolph Glacier Inventory v6 (2017); Table S2.1) from the 1 km resolution RACMO2.3 regional climate model (Noël et al., 2018) over the 2019 melt season as:

$$MF = \sum_{k=1}^{days} \sum_{j=1}^{Nsb} Sb$$

where *days* is the number of days since Julian day (JD) 182 (July 1st), *Nsb* is the number of daily RACMO2.3 grid cells showing negative balance, and *Sb* is the value of each 1 x 1 km grid cell. Values of *MF* were converted from centimeters to kilometers to provide a measure in gigatons of total melt. We assume that all melt is routed to the tidewater terminus where it enters the ocean.

As such, retention of meltwater within the remaining snowpack and / or firn is not accounted for in this study.

Independent validation of model performance over the Sverdrup glacier basin was performed by comparing spatially-coincident 1 km grid cells with *in situ* measurements of SMB as per Burgess (2018). Comparisons of cumulative surface mass balance (SMB) from RACMO2.3 with *in situ* measurements at each AWS (1 km resolution) provided daily validation of the intensity and duration of melt over the summer of 2019 as estimated from RACMO2.3 (Sup. Figure 2.2b and 2.2c). Results from these comparisons show that between measured and modeled SMB, RACMO2.3 results over-estimated summer melt by 20.4 mm w.e. at the SVD AWS and by 124 mm w.e. at the DICS AWS. It should be noted that the AWSs record single point measurements of ablation, while the RACMO2.3 data are averaged over 1km²; as such some discrepancy between measured and modelled values is expected. While both AWSs are situated in fairly different settings, i.e. DICS is exposed to high winds on the ice cap proper and the SVD station is relatively sheltered from the wind by the surrounding mountains in the Sverdrup glacier valley, both sites are situated on very shallow slopes, (<1°). AWS locations are also both characterised by relatively low relief (<0.5 m) sastrugi (wave-like features in snow caused by wind erosion) during the winter months. A higher degree of spatial variability occurs at SVD station during the summer months where surface ponds, stream channels and cryoconites are more common than at the higher elevation DICS. Reduced albedo due to the presence of these features could account for the bias towards higher estimations of modelled melt than was measured at the SVD station. Uncertainty of the total melt discharge from the Sverdrup glacier basin in 2019 as modelled by RACMO2.3 was assessed through comparisons with melt/accumulation measured at each stake in the Sverdrup glacier basin over the period from 2008 to 2015. The standard deviation of the differences between

RACMO2.3 and *in situ* measurements averaged for all stakes indicate an uncertainty of 120 mm w.e., with better agreement (± 90 mm w.e.) at higher elevations (≥ 1200 m a.s.l.) than at lower elevations (± 110 mm w.e. at ≤ 400 m a.s.l.). This standard deviation corresponds to an uncertainty of 0.1 Gt (Sup. Figure 2.2a) in modelled estimates of total meltwater flux from the Sverdrup glacier basin.

3. Results

3.1. Meltwater export

AWS and RACMO2.3 SMB data provide context for the timing and volume of meltwater exported from Sverdrup in 2019. AWS data confirms that the spring season glacial samples were collected pre-melt (Julian Days 94-132, Figure 2.2 blue box) and that summer season samples were collected during peak melt (Julian Days 209-227, Figure 2.2 red box). The net SMB directly measured at both AWSs and at 43 ablation stakes from 2008-2015 are consistent with previous work comparing RACMO2.3 results to SMB in the CAA (Burgess, 2018) and are in agreement with past assessments of RACMO2.3 SMB, where errors between measured and modeled melt were generally good ($\pm 4\%$), except for terminus regions on Agassiz, Devon, and Penny ice caps in the CAA (Noël et al., 2018). RACMO2.3 data from 2018-2019 for the Sverdrup watershed shows 0.34 Gt of summer melt over a 55 day melt season (Figure 2.2c). The first sign of summer melt (JD 154) was followed by ~ 10 days of net accumulation, with daily melt volumes peaking when the plume was first observed (Figure 2.2b). Summer field sampling took place during the second highest period of daily surface melt, and as sampling took place toward the end of the melt season, cumulative surface melt was near its highest.

The time-lapse camera (TLC) imagery and field observations at Sverdrup's terminus provide an independent and complementary characterization of the seasonal timing and characteristics of the turbid meltwater plume released at the ice front in 2019. These images and observations showed two persistent patches of turbid water in front of the terminus, one smaller and one larger, which were interpreted as the signatures of freshwater subglacial plumes rising to the surface. The main plume appeared to be discharged on the western side of the glacier, while a smaller plume was evident on the eastern side. TLC images showed that the first signs of summer melt (Julian Day 154, Figure 2.2b blue box) and plume development (Julian Day 194 Figure 2.2b red box) occurred on June 3 and July 13 (2019), respectively. Sup. Figure 2.3 shows results of the k-means pixel classification and an example image from the data set. Detected plume area was correlated with modeled cumulative surface mass balance (i.e. plume area increased as Sverdrup glacier lost mass over the melt season) from the AWS ($r=-0.71$, $p=0.015$, Sup. Figure 2.3c). This correlation gives confidence that detecting plume areas using this method is reasonable.

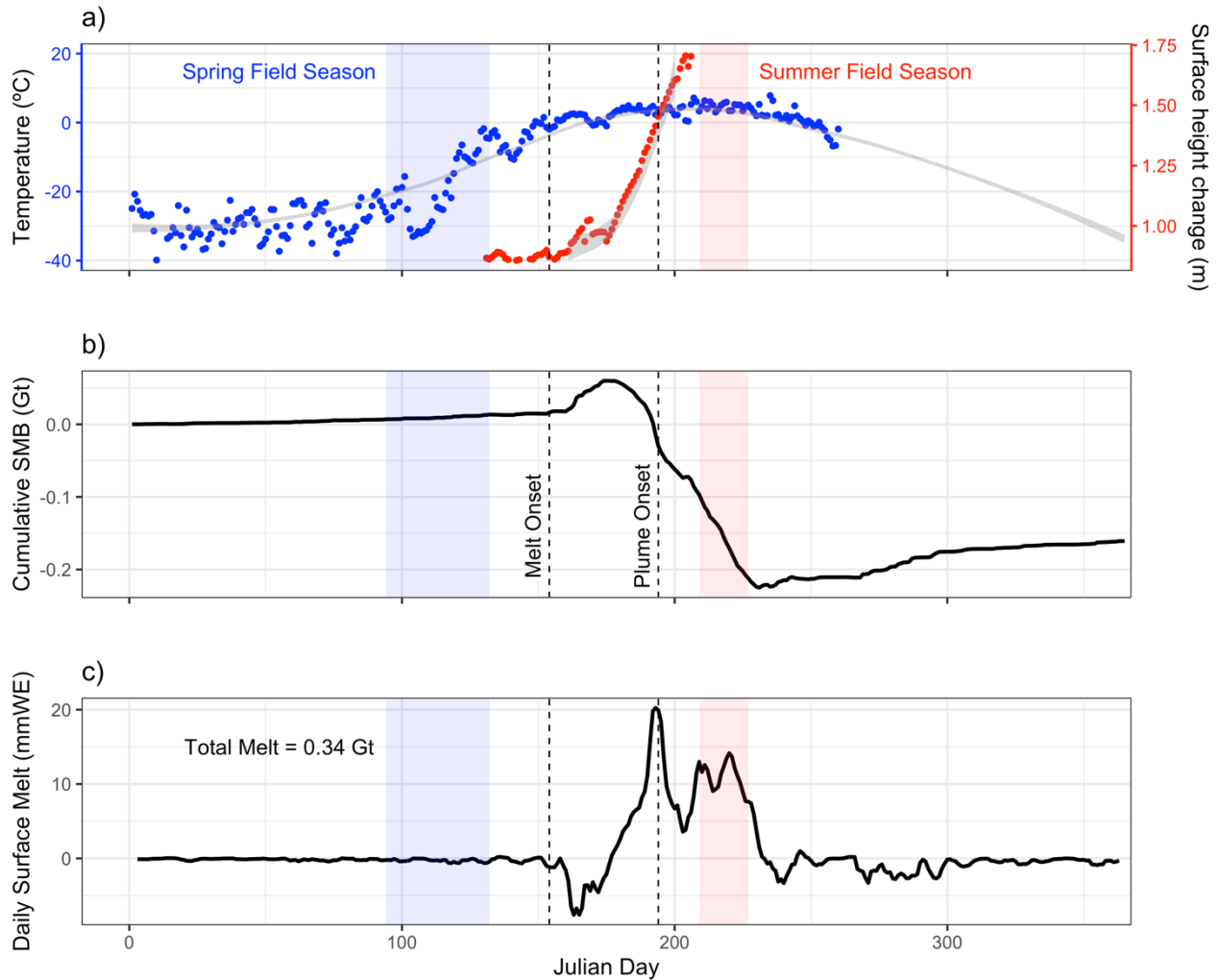


Figure 2.2. Sverdrup mass balance summary.

(a) Temperature (blue) and surface height change (red) data from SVD AWS. Gray fill represents the 95% confidence interval of 2016-2018 temperature and surface height change AWS measurements. (b) Daily and (c) cumulative 2019 RACMO2.3 surface mass balance data for Sverdrup Glacier. Melt and plume onset dates determined using time lapse camera imagery (black dotted lines) and the duration of the spring and summer 2019 sampling periods (blue and red shading) are shown in all panels.

3.2. Meltwater nutrient delivery

Analyses of on-ice and marine bottle samples for nutrient concentrations gives insight into the role of glacial discharge in the direct delivery of chemical species to the marine environment. Table 2.1 shows a summary of macronutrient (NO_3^- , PO_4^{3-} , SiO_4^{4-} , NH_4^+) and TDN concentrations

for glacial and marine samples. Marine samples are summarized for both the upper (≤ 40 -m depth) and deep (> 40 -m depth) water column in both relatively close proximity to the glacier front (≤ 4 km) and beyond 10 km from the glacier terminus. “Spring Glacial” samples represent a variety of glacial environments (i.e., basal ice, supraglacial snow, supraglacial ice, and overwinter water) while “Summer Glacial” samples consist of marginal runoff and supra- and subglacial melt. Geochemically, spring glacial samples had higher macronutrient concentrations and fluxes compared to summer glacial samples, indicating that the export of macronutrients to the marine environment may have significant seasonal variability. In contrast, DON did not vary significantly with season. The lower concentrations of macronutrients in summer glacial samples likely reflect shorter retention and rock-water interaction times and the absence of snow in late-season melt (Nienow et al., 1998; Richards et al., 1996; Wolff, 2013). A higher degree of variability in spring relative to summer glacial samples likely reflects the diversity of sample types collected. Concentrations of macronutrients, except for ammonia, were all lower in glacial samples compared to deeper marine (> 40 -m depth) samples.

Table 2.1. Glacial freshwater and marine seawater values.

Average and standard deviations for biogeochemical parameters (BLD = below limit of detection). Average values are given for marine depths as indicated. Samples ≤ 4 km from Sverdrup's terminus are within the moraines surrounding Brae Bay. The number of samples, (n) is also given.

Table 2.1		NO ₃ ⁻	PO ₄ ³⁻	SiO ₄ ⁴⁻	NH ₄ ⁺	TDN	$\delta^{18}\text{O}$	DOC	Chl <i>a</i>
	n	μM	μM	μM	μM	μM	‰	μM	$\mu\text{g/L}$
Spring Glacial	10	2.2 ± 0.3	0.3 ± 0.0	5.0 ± 0.2	1.4 ± 0.1	1.8 ± 0.2	-27.8 ± 0.4	16.4 ± 1.1	
Summer Glacial	11	1.8 ± 0.0	0.1 ± 0.0	*BDL	1.2 ± 0.0	1.8 ± 0.0	-26.7 ± 0.2	10.9 ± 0.4	
Marine ($\leq 40\text{m}$, $\leq 4\text{km}$)	18	2.0 ± 1.8	0.5 ± 0.2	5.6 ± 3.4	1.5 ± 1.8	5.64 ± 2.8	-3.0 ± 1.0	63.9 ± 44.2	2.2 ± 2.4
Marine ($\leq 40\text{m}$, $> 10\text{km}$)	6	1.4 ± 2.2	0.5 ± 0.3	4.2 ± 4.2	0.9 ± 0.5	5.8 ± 2.4	-2.0 ± 0.2	97.7 ± 40.8	1.6 ± 1.5
Marine ($> 40\text{m}$, $\leq 4\text{km}$)	3	6.6 ± 0.2	0.9 ± 0.1	12.9 ± 0.3	0.3 ± 0.5	12.2 ± 1.3	-1.7 ± 0.0	126.9 ± 20.7	0.1 ± 0.1
Marine ($> 40\text{m}$, $> 10\text{km}$)	7	6.5 ± 3.1	0.7 ± 0.1	11.1 ± 3.4	1.8 ± 1.2	10.5 ± 5.9	-1.3 ± 0.7	78.6 ± 26.6	0.4 ± 0.5

3.3. Meltwater carbon delivery

In addition to the potential for delivering nutrients, glacial discharge may also impact downstream carbon availability via the delivery of DOC in meltwater. Average and standard deviation DOC concentrations in spring and summer glacial samples as well as marine samples are shown in Table 2.1. Similar to macronutrient concentrations, there was more variability in DOC concentrations in spring glacial samples compared to summer samples, likely representing the larger variety of different sample types collected during the spring season. Further, also as with macronutrient concentrations, DOC concentrations in meltwater in both seasons were universally lower than marine concentrations. Given this, it appears that Sverdrup glacier does not export DOC in concentrations high enough to significantly augment DOC concentrations in the marine environment.

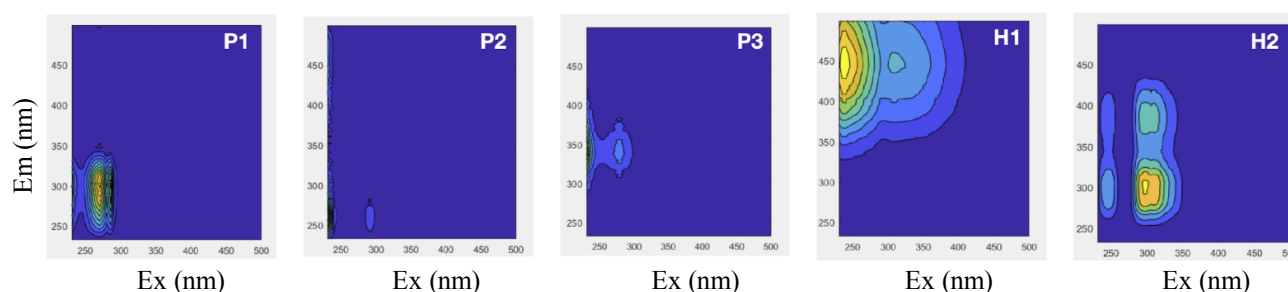
Though spring and summer glacial DOC concentrations were lower than those in marine samples, PARAFAC results show that the type of carbon present in spring and summer glacial

water was significantly different than in marine waters; we thus explored the generalized DOM component composition of glacial and marine samples to gain insight into the possible influence of glacial input on DOM in the near-shore marine environment. A five-component PARAFAC model applied to all spring glacial, summer glacial, and marine samples explains 97.73% of the variance in the dataset. The loading patterns of the five modeled components can be matched to previously-described fluorescent DOM fingerprints in glacierized environments (Table 2.2). P1 (tyrosine) and P2 (tryptophan) match protein-like peaks identified in marine and terrestrial samples from around the world (Coble, 1996) and broadly indicate autochthonous production of DOM (Stedmon & Markager, 2005). P3 has been found in glacial ice and meltwaters from the McMurdo Dry Valleys (Antarctica) as well as on Axel Heiberg and Ellesmere Islands in the CAA (Dubnick et al., 2017; Pautler et al., 2012). Components H1 and H2 are similar to previously described humic-like peaks. H1 is similar to a humic-like component of terrestrial origin ubiquitous to a wide range of natural catchments during the warmer months of the year and generally absent in wastewater (Stedmon et al., 2007). H2 is similar to the classic M peak (Coble, 1996) and has been defined as a marine humic-like component. Respectively, spring and summer glacial samples contained >40% and ~18% more protein-like components than marine samples. In contrast, marine samples had >60% more humic-like DOM compared to summer glacial samples and >300% more humic-like DOM relative to spring glacial samples. Though bulk DOM concentrations in glacial melt were not high enough to significantly increase marine concentrations, proportionally, there was significantly more protein-like DOM in glacial melt vs. in marine waters, with more protein-like DOM in spring glacial melt compared to summer meltwater. There was also a higher fraction of the P1 component (associated with summer glacial melt) in marine samples with higher turbidity compared to marine samples outside the turbid meltwater plume. It thus appears that the freshened

and turbid submarine meltwater plume delivers protein-like DOM to the surface of Brae Bay with a carbon signature similar to summer meltwater. This may be significant because secondary producers (marine heterotrophs) could benefit from this addition of bioavailable carbon.

Table 2.2. A summary of the 5 PARAFAC components.

Components modeled using fresh and marine samples from Sverdrup Glacier and Brae Bay (n = 55). Described here are wavelengths (nm) of the component excitation (Ex) and emission (Em) spectral peaks, the potential carbon source (protein-like vs. humic-like), and examples of previous studies that have found similar peaks in similar environments.



	Ex:Em (nm)	Potential Carbon Source	Literature Examples
P1	270: 301	Protein-like (Tyrosine)	Stedmon, 2005; Walker, 2009; Fellman, 2010
P2	290: 265	Protein-like (Tryptophan)	Coble, 1996; Walker, 2009; Fellman, 2010
P3	280: 337	Protein-like (autochthonous DOM via microbial degradation)	Coble, 2007; Pautler, 2012; Dubnick, 2010
H1	235, 310 : 441	Ubiquitous humic-like	Stedmon, 2005; Stedmon, 2007; Dubnick, 2010
H2	245, 295 : 300, 395	Marine humic-like, microbial degradation	Coble, 1996; Walker, 2009

To further assess seasonal and spatial differences in fluorescent DOM composition, a principal component analysis (PCA) was conducted using the relative abundance of the 5 modeled PARAFAC components (Figure 2.3). The first and second principal components described 58.7% and 20.4% of the variance in the normalized PARAFAC dataset, respectively. PCA results show a clear differentiation between glacial and marine samples and between the spring and summer glacial samples. A PERMANOVA test confirms that these clusters are significantly different (p

<0.004) while the ANOVA f-test ($f > 10^{20}$) confirms that this difference is due to between-group variability. P1 and P3 are associated with spring melt, P2 is associated with summer melt, and H1 and H2 are associated with summer marine samples. This analysis confirms the unique DOM signatures of the glacier meltwater relative to the marine waters, and further the seasonal evolution of meltwater DOM characteristics.

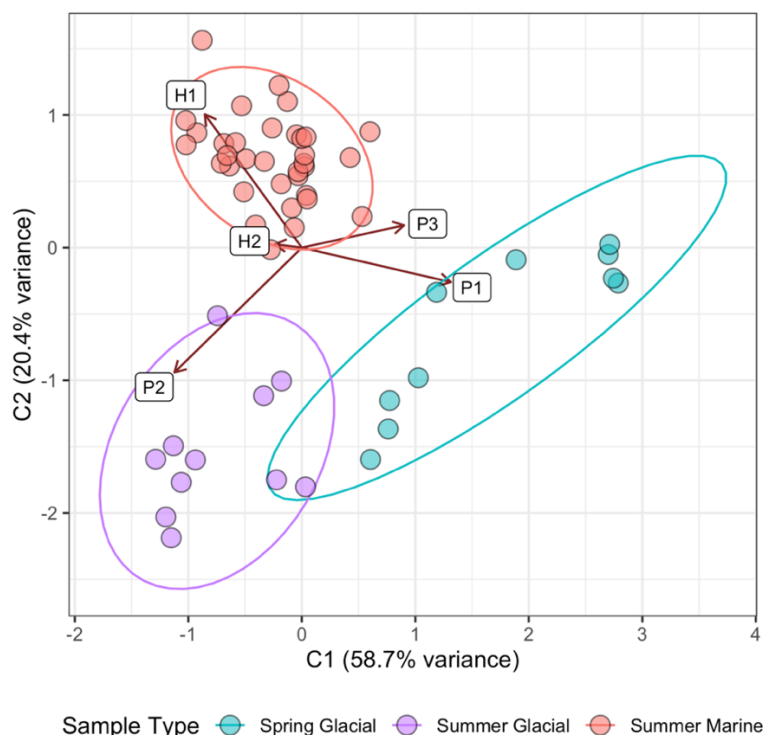


Figure 2.3. Principal component analysis (PCA) of the five modeled PARAFAC components. Data is grouped by season (spring vs. summer) and water type (glacial vs. marine). A PERMANOVA test ($p < 0.004$) confirms these clusters are significant while the ANOVA f-test ($f > 1020$) confirms that this significance is due to between-group variability.

3.4. Glacial meltwater in the near-shore marine environment

The fate of glacial meltwater in the marine environment is mapped by measurements of $\delta^{18}\text{O}$, salinity, oxygen, and turbidity in marine water sampled at various locations relative to the

glacier terminus. Specifically, marine profiles along the “near” (~0.8 km from the ice terminus), “distal” (~2.5 km from the ice terminus), and “out” (from within 1-km to more than 25 km from the ice terminus) transects suggests that glacial meltwater is largely confined to the upper 30-40 m of the water column, directly impacting waters ≤ 4 km from the glacier front. Marine water column profiles show a spatial gradient in $\delta^{18}\text{O}$ (Figure 2.4a), salinity (Figure 2.4b), dissolved oxygen (Figure 2.4c), and turbidity (Figure 2.4d), with fresher, more ^{18}O -depleted, oxygen-rich, and turbid waters found closer to the ocean surface and the calving front. ^{18}O -depleted water is characteristic of glacial meltwater due to Rayleigh fractionation (Tranter, 2011). The “out” transect (Figure 2.4) shows a clear spatial correlation between ^{18}O -depletion (glacial melt) and areas of low salinity, high dissolved oxygen, and high turbidity – all indicators of glacially-impacted waters. For all samples, water deeper than 10 m was less depleted in ^{18}O (average $\delta^{18}\text{O}$: -1.75‰) than water above 10 m (average $\delta^{18}\text{O}$: -3.45‰). Further, surface (≥ 10 m depth) samples of the “near” transect (Figure 2.5, top) were more depleted in ^{18}O (average $\delta^{18}\text{O}$: -4.24‰) than the “distal” transect (Figure 2.5 bottom, average $\delta^{18}\text{O}$: -3.42‰), which in turn were more depleted than surface samples collected >10 km from shore outside of the ring of moraines enclosing Brae Bay (average $\delta^{18}\text{O}$: -2.18‰). These values indicate a glacial meltwater signal in the marine environment which appears to be largely confined to upper 30-40 m of the water column and quickly diluted within 4 km of calving front. Rising submarine discharge plumes can be patchy (Andersen et al., 2010; Everett et al., 2018; Jackson et al., 2017), but using turbidity as an indicator, the plume can be detected as far out as station 27, ~3.7 km from Sverdrup’s terminus (Figure 2.4d). Turbidity thus corroborates the $\delta^{18}\text{O}$ picture of meltwater impacting waters primarily within 4 km from the glacier front. CTD sensor measurements of dissolved oxygen provide a more highly-resolved view of the potential meltwater plume and further show an extended glacial influence: a “plume-like” region of elevated

dissolved oxygen concentration is observed within the top 20 m of the water column and extends to station 31, ~13 km from the terminus (Figure 2.4c). In the “near” and “distal” transects (Figure 2.5c) there is evidence of a subsurface plume with elevated dissolved oxygen concentrations centered at ~12 m depth in the "near" transect, which rises (centered ~10 m depth) and dilutes/disperses in the "distal" transect.

The mapped density structure indicates that the meltwater, which enters the marine environment at depth, rises to the surface within 4 km of Sverdrup’s terminus. The "plume-like" feature seen in $\delta^{18}\text{O}$, salinity, dissolved oxygen, and turbidity follow the $>1025 \text{ kg m}^{-3}$ isopycnal which slopes upwards from the terminus within the first 4 km of the “out” transect (Figure 2.4, Station 22-30, white lines). Upsloping isopycnals associated with the plume along this transect (i.e. those associated with densities $\leq 1026 \text{ kg m}^{-3}$) begin at depths ≥ 30 m depth (Figure 2.4); by linearly extrapolating these lines of equal density back to the terminus, it appears that the plume originates from depths between 30-40 m.

A two-component mixing model using summer marginal melt and Jones Sound deep water as end-members (Sup. Table 2.1) was constructed to quantify the fraction of glacially-derived water in marine samples and to track its extent in the near-shore environment. The model uses $\delta^{18}\text{O}$ and salinity values of the most ^{18}O -depleted marginal runoff summer sample (Sup. Figure 2.4, “MR”) and $\delta^{18}\text{O}$ and salinity values of the most ^{18}O -enriched deep marine sample (Sup. Figure 2.4, “JS”) to calculate the fraction of glacial melt in all marine samples (Figure 2.6). Calculations of glacial meltwater fraction are based on similar work done by Östlund and Gert (1984) and Kanna et al. (2018). Surface waters (≥ 10 m) in the “near” transect have the highest meltwater fractions (~12% glacial melt and ~88% marine water on average). However, even these fractions are low and the surface plume water contains significant amounts of marine water even in the freshest part

of the sampled plume. The meltwater fraction declines with depth, where subsurface water (10-40 m below surface) averaged ~6% glacial melt, while deep waters (>40 m below surface) contained <5% glacial melt (Figure 2.6). Glacial melt fraction declines with distance from the glacier terminus; surface water within 4 km of shore was ~12% melt, while the average melt fraction >4 km from shore at the surface was ~7%. Overall the model suggests the plume, as sampled, is diluted with marine water even at close proximity to the terminus; further it suggests glacial melt primarily impacts near-surface waters and is diluted/dispersed efficiently with distance from the terminus.

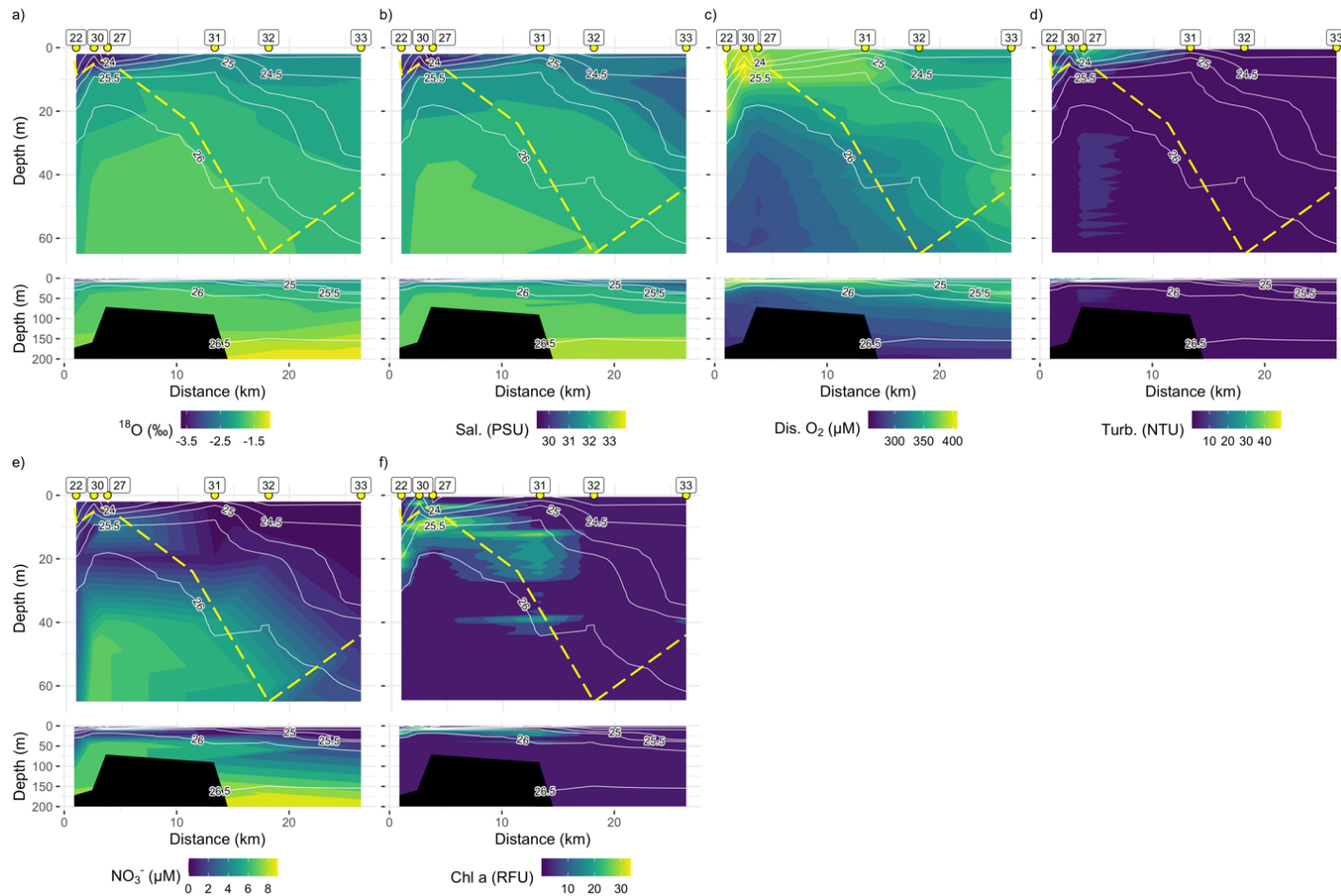


Figure 2.4. Plots of (a) $\delta^{18}\text{O}$, (b) salinity, (c) dissolved oxygen concentration, (d) turbidity, (e) nitrate concentration, and (f) Chl *a* concentration along the “out” transect in Brae Bay.

Density anomaly (kg m^{-3}) contours are shown in white. The dotted yellow line represents euphotic depth, calculated at 0.1% of surface PAR. Only the NO₃⁻ concentration profile is shown, but PO₄³⁻ and SiO₄⁴⁻ concentrations follow similar patterns. Station numbers are indicated at the top of the plot and distance is defined as starting at the glacier calving front. Bathymetry data (black) is from echo soundings made at each station.

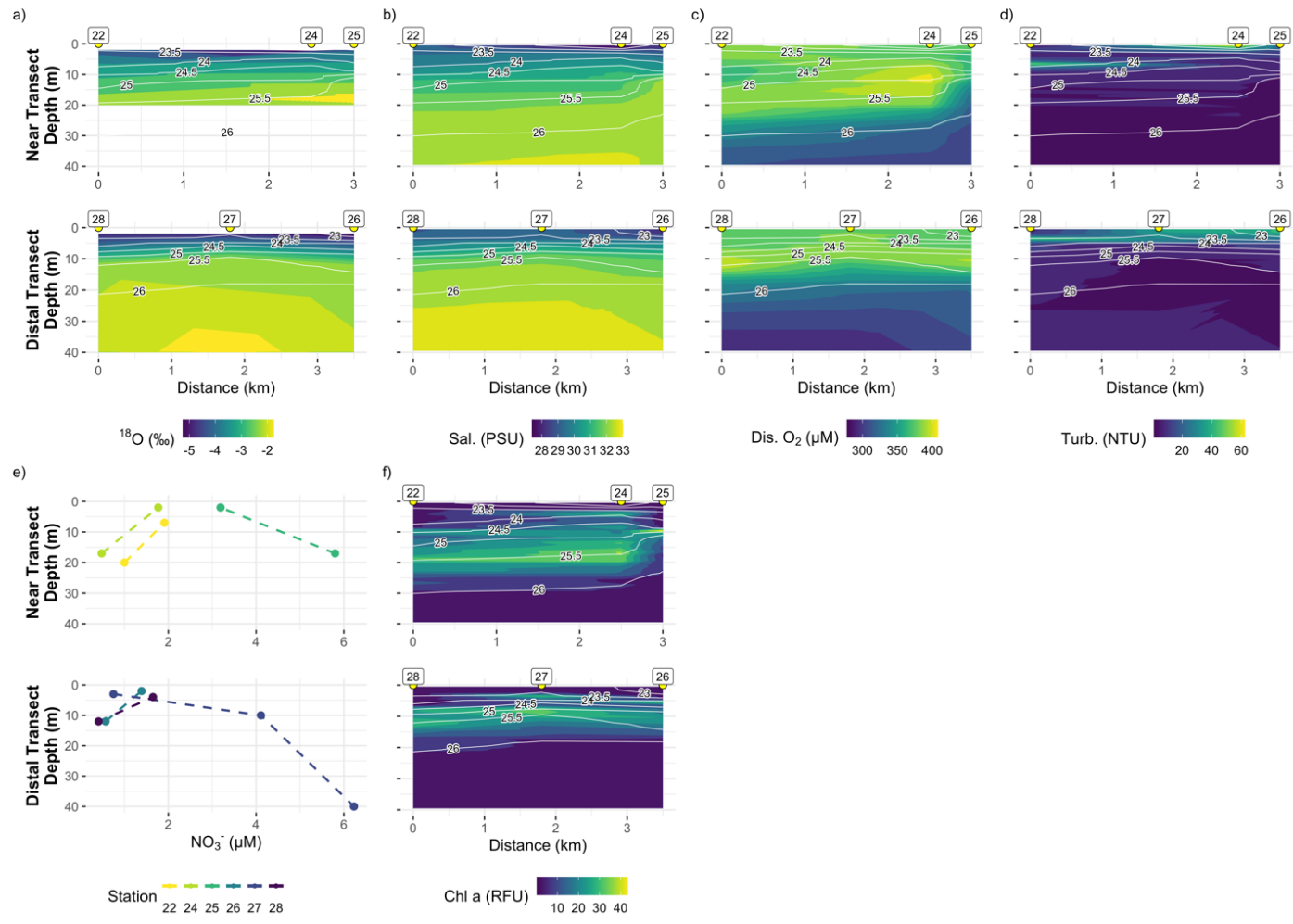


Figure 2.5. Plots of (a) $\delta^{18}\text{O}$, (b) salinity, (c) dissolved oxygen concentration, (d) turbidity, (e) nitrate concentration, and (f) Chl *a* concentration along the “near” (top) and “distal” (bottom) transects in Brae Bay.

Density anomaly (kg m^{-3}) contours are shown in white. Only the NO_3^- concentration profile is shown, but PO_4^{3-} , and SiO_4^{4-} concentrations follow similar patterns. Station numbers are indicated at the top of the plot and distance is defined as starting at the first station along the lateral transect.

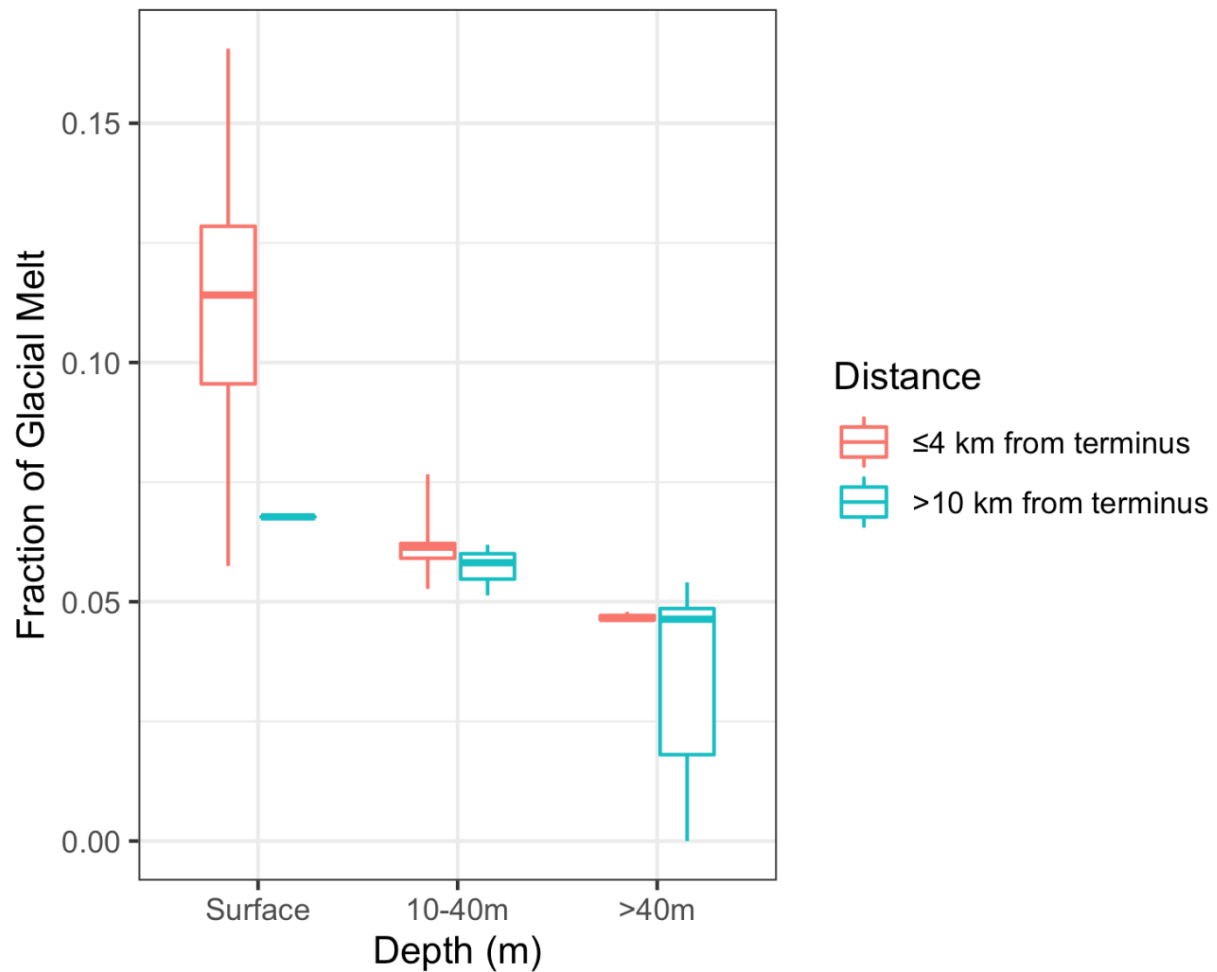


Figure 2.6. Boxplot of glacial melt fractions for all samples.

The median and interquartile range for each water type are shown for marine surface water (0-10m depth), marine near-surface water (10-100m depth), and marine deep water (>100 m depth). Colors denote distance away from Sverdrup glacier's terminal ice edge.

3.5. Meltwater impacts on the marine environment

Finally, the impacts of glacial input on nutrient availability, light availability, and primary production are explored via marine water column measurements. Although nutrient concentrations in glacial vs. marine samples (Table 2.1) show that glacial meltwater does not significantly impact near-terminus marine water nutrient concentrations, marine measurements suggest that glacial input at Sverdrup glacier does drive the delivery of marine-sourced nutrients from deeper water to

the near-surface. This delivery likely occurs via entrainment in the rising meltwater plume and/or the estuarine upwelling circulation forced by the glacier's freshwater input. The mapped density structure (Figure 2.4, white contours) indicates that isopycnals in the density range of 1025-1026 kg m⁻³ slope upwards towards the glacier terminus starting >26 km from the glacier. This structure provides an adiabatic pathway for marine waters at depths >60 m in the open waters of Jones Sound to upwell to depths of 5-10 m in near-coastal waters in close proximity to the glacier terminus. Nutrient concentrations (nitrate, phosphate, and silicate) are generally lower at the surface and higher at depth (Table 2.1) as is typical in marine waters in the late Summer (Randelhoff et al., 2020). Thus, the upwelling implied by the isopycnal structure likely plays a role in delivering marine waters with significant major nutrient concentrations to the near-surface. Measured nutrient concentrations (Figures 2.4e, 2.5e) are consistent with this scenario: nitrate concentrations are enhanced on the underside of the rising meltwater plume at concentration levels consistent with those of the 1025-1026 kg m⁻³ density classes. The entrainment observed at Sverdrup glacier is shallow compared to that observed at deep tidewater glaciers in Greenland (Kanna et al., 2018; Meire et al., 2017) but nevertheless appears important for enhancing nutrient concentrations: nutrient samples indicate that the nutricline (defined here as the depth where NO₃⁻ concentrations exceed 1-μM) at all the stations within Brae Bay (≤10 km of the glacier terminus) occurs at or above 30 m depth. Further, average NO₃⁻ concentrations in the upper 100 m of the “out” transect were higher at stations within Brae Bay (stations 22, 30, 27) than those farther out in Jones Sound (stations 30, 31, 32).

The conclusion that nutrients present in near-surface waters in close proximity to the glacier terminus are marine – as opposed to glacier-sourced – is further supported by the observed linear relationship between nutrient concentrations and AOU. The relationship between nutrient

concentrations and AOU can be used to determine if marine nutrient concentrations are being impacted by direct addition of glacially-derived nutrients, as such a ‘disturbance’ to a water mass is expected to cause a departure from a linear relationship. In this system, nitrate, phosphate, and silicate concentrations show linear relationships with AOU in both surface and subsurface water throughout Sverdrup Bay (Figure 2.7a,b,c), as expected for nutrients that are deep water-sourced. Expectedly, turbidity does not show this linear relationship, as turbid waters in this system are glacially-sourced (Figure 2.7d).

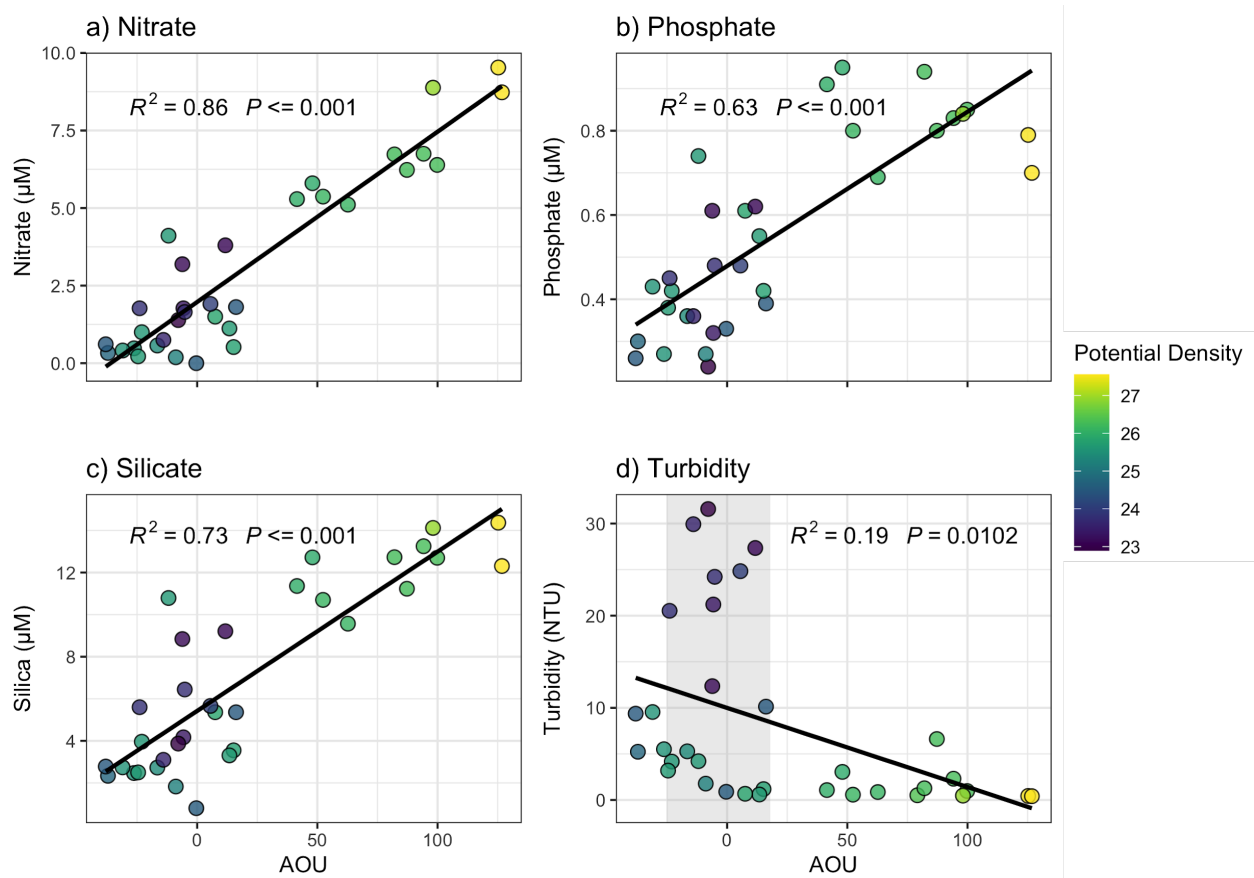


Figure 2.7. Apparent oxygen utilization (AOU) versus (a) NO₃⁻, (b) PO₄³⁻, (c) SiO₄⁴⁻, and (d) turbidity of marine water in Sverdrup Bay.

The colour scale shows the log of depth (m). The AOU range of plume water in (d) is shown in grey.

A second important impact of glacial input on the marine environment is its impact on light availability in near-surface coastal waters in close proximity to the glacier terminus. The export of sediment-laden glacial runoff from Sverdrup Glacier into Jones Sound leads to areas of high turbidity and low light availability in the upper ~10m of the water column close (<4 km) to the freshwater outlet at the glacier terminus (Figures 2.4d and 2.5d). As a consequence, the euphotic zone (Figure 2.4, above the yellow dotted line) in close proximity to the terminus is influenced significantly: at station 22 (that closest to the glacier terminus) the euphotic zone depth was 9 m and it decreased to less than 5 m at stations 30 and 27 as the buoyant turbid plume rose towards the surface with distance offshore. Consistent with other indicators of the meltwater plume, which suggest that the plume is quickly diluted within 4 km of the calving front (Section 3.4), euphotic zone depths increase to over 20 m beyond a distance of ~4 km from the ice front.

Glacially-induced nutrient entrainment and elevated turbidity limiting light available in close proximity (within ~4km) of the terminus are likely to impact primary production in these waters, although the combined net influence is not straight-forward to predict. On a large scale, elevated near-surface Chl *a* concentrations were found at stations closest to the glacier front and declined with depth and distance away from the glacier terminus: on average, higher Chl *a* concentrations were present at all three “near” stations compared to stations on the “distal” transect (Figure 2.5f) and Chl *a* concentrations were higher at “near” and “distal” transect stations than at stations further from shore along the “out” transect (Figure 2.4f). On a smaller scale, relationships between Chl *a* concentration, turbidity, and nutrient concentrations were variable. Consistent with expectations, the least turbid and most nutrient-rich (~6 $\mu\text{M NO}_3^-$) “near” station (station 25) had the highest Chl *a* concentration (>40 RFU from CTD data). However, at many stations close the glacier front (e.g. stations 22, 24, 27, and 30) the highest Chl *a* concentrations (30-40 RFU from

CTD data) were measured below regions of high turbidity despite the impacts of the turbid plume limiting light (Figures 2.4d,f and 2.5d,f). Peaks in Chl *a* concentration at stations 22, 24, 26, 28 and 30 coincide with lower nutrient concentrations, while stations 25 and 27 have elevated Chl *a* and nutrient concentrations (Figures 2.4e,f and 2.5e,f).

4. Discussion

4.1. Plume dynamics in the near-shore environment

At Sverdrup Glacier, a shallow, warm-based tidewater glacier in the CAA, time-lapse camera imagery (Section 3.1) and *in situ* marine observations (Section 3.4) confirm the existence of a freshwater plume in the near-shore marine environment tied to the glacier melt season evolution. Unsurprisingly, the correlation between plume area and cumulative mass balance (Sup. Figure 2.3) suggests that plume surface area is tied to the total volume of melt coming from the glacier. It can be inferred that as the melt season progresses, a larger area of marine waters in Brae Bay are impacted by glacial melt. *In situ* water samples in this study were collected when the cumulative meltwater flux was near its peak (late summer), and cumulative mass balance was at its most negative. It can be assumed that this sampling reflects a time of year when meltwater extent in Brae Bay was likely near its maximum.

Results suggest that meltwater exits Sverdrup's terminus 10's of meters below the sea surface. A single on-ice transect from 2009 showed the grounding line within 0.6 km of the terminus to be 20 ± 10 m below the surface (Larsen, 2010). Subsequent erosion caused by continued subglacial drainage likely results in the plume now exiting at even greater depth (Anderson et al., 2006; Catania et al., 2018; Kessler et al., 2008). Additionally, the ice elevations off the centerline are more than 10 m lower than the measured transect. These lower ice surfaces

are around a tunnel where subglacial melt was observed in 2019 to exit into Brae Bay (Sup. Figure 2.1b). This depression suggests that discharge is exiting Sverdrup Glacier at a depth of >30 m on the eastern side of the terminus where the main plume was observed in 2019 (Figure 2.1c).

The injection of the subsurface meltwater plume has important implications for water column structure in the ocean near the glacier front (Section 3.4). Near-surface (≤ 30 m depth) isopycnals within 4 km of the terminus slope upwards away from the terminus, mapping the rise of the buoyant plume to the surface between stations 22 (<1 km distance) and 31 (~ 13 km distance). The plume's influence appears to extend down to the $1026 \text{ kg m}^{-3} \sigma_{\theta}$ isopycnal, and extrapolation of this isopycnal's slope to the terminus indicates that the plume is originating from below 40 m depth, consistent with Sverdrup's estimated grounding line depth at this point along the terminus (≥ 30 m depth). This location also corresponds to the location of the main plume discharge that was observed in 2019. Further offshore between 13 and 26 km from the terminus (at stations 31, 32 and 33), isopycnals slope upwards towards the shore, characteristic of fjord-estuarine circulation. Here, the upward-sloping isopycnals begin outside the ring of moraines that hem in Brae Bay, therefore it is unlikely that this upwelling is driven directly by submarine glacial discharge solely from Sverdrup Glacier. Rather, this distal upwelling could be driven by variations in bathymetry (data not collected) between 4-10 km from the terminus (Timmermans & Marshall, 2020) or wind-driven Ekman transport in Jones Sound (Dmitrenko et al., 2016; Woodgate et al., 2005). Regardless of the forcing, this upwelling of deeper waters originating from Jones Sound has important implications for nutrient transport (Section 4.5).

4.2. Nutrient and carbon export in glacial meltwater runoff to the surface ocean

It has been proposed that glacial meltwater can be a primary mechanism for the delivery of macronutrients to the ocean (Hawkings et al., 2016; Hawkings et al., 2017; Tranter et al., 2002). Our results suggest however that at Sverdrup Glacier in summer the concentrations of macronutrients in glacial meltwater runoff were not high enough to significantly augment marine concentrations. Specifically, phosphate and silicate concentrations in glacial runoff were lower than in marine water samples (Table 2.1). While average summer glacial and upper (>40 m depth) marine water column nitrate concentrations were not significantly different (Table 2.1), the volume of freshwater exported from Sverdrup Glacier over the melt season (0.34 Gt; Section 3.1) is small compared to the reservoir of receiving seawater. RACMO2.3 model results suggest that on average 5.8×10^9 L of glacial melt are delivered to the ocean each day over the 55 day summer melt season (Figure 2.2). Given the average nitrate concentrations in summer meltwater of $1.8 \pm 0.0 \mu\text{M}$ (Table 2.1), this implies an average daily nitrate delivery rate of $(1.1 \pm 0.2) \times 10^4$ mol per day. Accounting for summer plume extent, this delivery rate is estimated to impact a minimum volume of ~ 0.01 km³ of ocean water. Thus, even under the assumption of no biological uptake of nitrate, the glacial melt delivery rate is an order of magnitude too small to account for the observed 0.6-1.9 μM nitrate found in the upper 10 m of the marine water column at stations affected by the plume (Figures 2.4 and 5). Collectively, these results suggest that glacial melt from Sverdrup Glacier does not appreciably augment existing macronutrient concentrations in the coastal ocean distal to the ice front.

This conclusion agrees with recent studies that found direct addition via glacial meltwaters to not be a primary mechanism for delivery of macronutrients to the ocean (Cape et al., 2018; Kanna et al., 2018; Meire et al., 2017). However, debate remains, and seasonality and hydrology

appear to play important roles in carbon and nutrient availability (Beaton et al., 2017; Hawkings et al., 2017; Hopwood et al., 2020). In the case of NO_3^- , a large fraction of glacially-sourced NO_3^- is derived from atmospheric deposition on the surface snowpack (Wolff, 2013), and because snow is the first to melt in summer, most of this NO_3^- is exported early in the season (Wadham et al., 2016). For example, Wadham et al. (2016) found significant concentrations of NO_3^- ($>4 \mu\text{M}$) in runoff rivers draining Leverett Glacier in samples collected before June, but by late July, NO_3^- concentrations were comparable to average concentrations observed on Sverdrup Glacier ($\sim 2 \mu\text{M}$). The low NO_3^- concentrations in the summer glacier meltwater found in this study are likely influenced by the time of sampling, i.e. at the peak of melt, when ice melt rather than snow melt dominates glacial runoff. However, should the seasonal variation of NO_3^- concentrations in meltwater from Sverdrup Glacier be of a similar magnitude to that of Leverett Glacier (~ 2 -fold difference in nutrient concentrations between early and late melt), we note that seasonal variation is still insufficient for direct NO_3^- delivery rates to account for the observed NO_3^- enrichment in the surface waters in Brae Bay. Further, we note that spring vs. summer glacial water samples from Sverdrup Glacier do not show a large difference in NO_3^- concentrations (Table 2.1).

In contrast, other studies of glaciers in Greenland have found glacial meltwater to be a significant source of crustal elements, including silica (Hawkings et al., 2017; Meire et al., 2016; Tranter et al., 2002) and phosphate (Hawkings et al., 2016), during peak meltwater flow. In the context of these studies, our findings of low silicate and phosphate concentrations in summer meltwater at Sverdrup Glacier are anomalous. The elevated concentrations of crustal elements seen in the Greenland glacier studies are likely the result of bedrock geology, a prolonged melt season and/or longer subglacial hydrological flow-paths, the latter two of which can result in extensive water–rock interaction and enhanced physical and biologically-mediated weathering (Aciego et

al., 2015; Ravier & Buoncristiani, 2018). The Canadian Shield underlies both eastern Devon Island and Greenland, so it is unlikely that fundamentally different bedrock geologies are the cause of the variation in these macronutrient concentrations between Sverdrup Glacier and the glaciers studied in Greenland. Instead, it is more likely that glacier hydrology and meltwater routing played a role in generating the low meltwater nutrient concentrations observed in this study (Brown, 2002). Similar to previous work (Hawkings et al., 2017; Meire et al., 2017), meltwater samples here were collected in late summer, when basal hydrology is characterized by fast efficient export and short rock-water interactions, limiting enrichment of crustal elements in the meltwater. Phosphate and silicate concentrations in frozen spring samples were significantly higher than in the summer (Table 2.1), and thus, these lower crustal nutrient concentrations in summer melt may be evidence of low contact times. Further, on Sverdrup Glacier, most glacial melt is routed marginally until just prior to the terminus. This marginal routing likely denotes significantly shorter rock-water interactions with the glacier bed, explaining the lower summer PO_4^{3-} , SiO_4^{4-} , and carbon concentrations observed (Bennett, 2011). Finally, Sverdrup Glacier's slow ice velocities may result in less basal erosion and a subsequent lack of crustal elements in meltwater. Indeed, Milner et al. (2017) proposed that as glaciers and ice caps shrink, the quantity of soluble reactive phosphorus exported in runoff decreases.

Similar to major nutrient concentrations, the concentration of glacial DOC was not high enough for glacier meltwater inputs to significantly augment marine concentrations (Table 2.1). However, as discussed in Section 3.3, glacier meltwater differed significantly from marine waters with respect to the types of carbon present, with potentially important implications for the bioavailability of DOM to support marine ecosystems. Specifically, meltwater runoff from Sverdrup Glacier had a higher proportion of protein-like DOM compared to the more humic-like

marine DOM and based on PARAFAC and PCA analyses, protein-like DOM components (P1-P3) were most associated with glacial samples. Tyrosine (P1) and tryptophan (P2) components were identified by Yamashita et al. (2015) to be indicators of the bioavailability of DOM in marine waters; this suggests that glacial samples from Sverdrup Glacier have a higher proportion of bioavailable protein-like DOM compared to marine water samples. The P3 component is related to the production of DOM via biological degradation; thus, the association between spring glacial samples and P3 we find could be an indicator that protein-like DOM is a result of microbially-mediated processes occurring in the basal and marginal environments (Smith et al., 2018). These three protein-like components have been previously found in DOM collected from Devon Island (Dubnick et al., 2017) and northern Alaska (Walker et al., 2009), as well as in riverine, and to a lesser extent estuarine, waters draining the Juneau Ice Field (Fellman et al., 2010b). As found in numerous other glacier studies, protein-like DOM in supraglacial and basal samples (>90% protein-like) is likely the result of productive microbial communities living on and under the ice that are able to generate and recycle bioavailable DOM for downstream export and consumption (Bhatia et al., 2010; Hood et al., 2009; Smith et al., 2018). The elevated ammonium concentrations observed here may also indicate microbial degradation of glacial DOM (Kumar et al., 2016). A recent study by Dubnick et al. (2020) corroborates this, having found abundant and distinct microbial communities in surface and basal ice at Sverdrup Glacier. The humic-like component H1 has been found in both marine and terrestrial studies (Coble, 2007; De Souza Sierra et al., 1994; Stedmon et al., 2003) and has been previously observed in basal ice from numerous glaciers on Devon Island (Dubnick et al., 2017). The marine humic-like component H2 has also previously been found in basal ice from Devon Island (Dubnick et al., 2017) and Alaska marine DOM (Walker et al., 2009). Broadly, the protein-like glacier DOM found in meltwater runoff draining Sverdrup

Glacier and the humic-like marine DOM found in the surrounding coastal ocean is consistent with previous findings, indicating that glaciers are microbially-based ecosystems capable of supplying comparatively labile DOM to downstream environments (Dubnick et al., 2020; Hood et al., 2009). In the ocean, this labile DOM in glacial melt can promote secondary productivity, with bacteria and microzooplankton using it as a carbon source. These organisms then go on to feed higher trophic levels in the marine food web (Pomeroy, 1974). Recent work in the McMurdo Dry Valleys (Antarctica) has found that heterotrophic production relies on labile DOM freshly-derived from photosynthetic bacteria rather than legacy organic carbon (Smith et al., 2017). While delineating the source of protein-like DOM in the ocean or its relative importance to CAA heterotrophs is beyond the scope of this study, if marine microbes preferentially use labile glacially-derived protein-like carbon over humic-like marine carbon, as has been found in previous studies in Alaska and Colorado (Arimitsu et al., 2018; Fegel et al., 2019; Fellman et al., 2015), tidewater glaciers like Sverdrup Glacier, which export labile DOM to the ocean, may play an important role in stimulating local secondary production in Arctic waters distal to the ice terminus during the summer months.

4.3. Impact of the submarine discharge plume on the surface ocean

While carbon and nutrient concentrations in glacial melt were not high enough to directly impact the marine environment, signatures of buoyant plume rising close to the terminus (within 4 km) and the upwelling of deeper marine waters consistent with an estuarine-like circulation farther out in Jones Sound (~13-23 km from the terminus) were both detected (Sections 3.4 and 3.5). In marine water unaffected by external nutrient sources, AOU will have a positive linear relationship with nutrient concentration because oxygen consumption and nutrient additions have

a shared source: organic matter remineralization. This linear relationship is observed in Brae Bay (Figure 2.7), further confirming that glacial melt is likely not the important source of the enriched macronutrient concentrations observed in marine waters surrounding Sverdrup Glacier.

Previous studies of glacier-induced upwelling focus primarily on the delivery of nitrate from depth, as NO_3^- is generally the limiting nutrient in the North Atlantic and Arctic oceans in the summer (Randelhoff et al., 2020). Nutrient ratios in Brae Bay suggest that surface phytoplankton are nitrogen limited at this time of year (Sup. Figure 2.5), and though upwelling at Sverdrup Glacier is shallow, it occurs below the nutricline (≥ 30 m depth) and is therefore sufficient to deliver waters with elevated nutrient concentrations ($\sim 5 \mu\text{M}$) to the surface. Recent studies of four tidewater glaciers (Kronebreen, Kongsvegen, Conwaybreen, and Kongsbreen) in Kongsfjorden (Svalbard) all with relatively shallow (≤ 70 m depth) grounding lines found similar upwelled NO_3^- concentrations ($4.2 \mu\text{M}$) (Halbach et al., 2019). In comparison, deep tidewater glaciers in Greenland have been shown to be capable of entraining marine water with nearly double the NO_3^- concentration ($\sim 10 \mu\text{M}$) that is observed here (Kanna et al., 2018; Meire et al., 2017). However, given that NO_3^- is limiting at this time of year following the spring bloom, the delivery of waters with even modest concentrations of NO_3^- to the euphotic zone may promote productivity. The analysis of glacial melt fraction (Section 3.4) indicated that the rising meltwater plume is $\sim 13\%$ glacial melt (87% marine water), and RACMO2.3 modeling (Section 3.1) predicted that over the melt season Sverdrup exports a total of 0.34 Gt of meltwater to Brae Bay. These estimates and measured NO_3^- concentrations thus imply that 2.0 Gt of deeper marine water and $>10^{15}$ mol of NO_3^- may be delivered to surface waters during the summer – compared to the <0.5 Gt of NO_3^- delivered in spring and summer glacial melt. If this delivery is typical of the over 300 tidewater glaciers in the CAA, this implies that tidewater glaciers in this region may be responsible for

delivering >3 Gt of NO_3^- to the surface ocean annually. It should be noted that the differences in underlying geology of CAA glaciers likely makes this estimation highly uncertain. Further, while most tidewater glaciers in the CAA have shallow discharge plumes relative to glaciers in Greenland, Sverdrup Glacier is an example of a very shallow tidewater glacier, even for the CAA (Cook et al., 2019), and thus, this estimate may likely be an underestimation. Regardless, this value represents nearly 2x more nitrate than is exported by the Mackenzie River in a year (Holmes et al., 2011). Note, however, that riverine input represents a source of ‘new’ nitrogen to the marine environment while glacially-derived upwelling redistributes marine nitrogen. Both are important for supporting productivity, but only ‘new’ nitrogen can alter the total marine nitrogen budget.

4.4. Glacier effects on primary productivity in front of a shallow tidewater glacier

Past studies of glaciers in Greenland and Svalbard have observed elevated surface concentrations of Chl *a* associated with regions of glacially-driven upwelling of nutrient-rich marine waters (Halbach et al., 2019; Kanna et al., 2018; Meire et al., 2017). Here, peaks in Chl *a* concentrations are primarily found within (stations 22, 30) or at the edges (station 24 and 25) of the turbid meltwater plume in Brae Bay (Figures 2.4 and 2.5). The presence of high Chl *a* concentrations in areas of low nutrient concentrations suggests the biological uptake of macronutrients. Higher Chl *a* concentrations at all three “near” stations compared to the stations on the “distal” and “out” transects suggest that the strongest biological response to the buoyant meltwater plume upwelling occurs within 1 km of the terminus, where entrained nutrient-rich marine water is delivered to the surface. We also observe elevated Chl *a* concentrations ~13 km from the terminus (station 31) in an area of upwelling of deeper marine waters outside of the moraines hemming Brae Bay. It is unlikely that this estuarine-like upwelling >10 km from

Sverdrup's terminus is wholly dependent on subglacial discharge exiting at ≥ 30 m depth from the terminus of Sverdrup Glacier, but freshwater delivery along the coast may play an important role in driving estuarine-like circulation. Regardless, the distal upwelling does appear to promote the delivery of nutrient-rich water to the surface farther out in Jones Sound, sustaining elevated Chl *a* concentrations compared to surface waters >20 km from Sverdrup.

The Chl *a* responses seen in the Sverdrup Glacier system differ from those reported in studies on larger Greenland glaciers in important respects; specifically, the response is less extreme and spatial extent more limited at Sverdrup Glacier. Maximum Chl *a* concentration at Sverdrup was ~ 7.5 $\mu\text{g/L}$ (extracted concentration), while concentrations in previous studies in Greenland can exceed 20 $\mu\text{g/L}$ (Meire et al., 2017). These relatively small Chl *a* enhancements appear consistent with shallower tidewater glacier systems. Recent work at shallow tidewater glaciers in Svalbard report maximum Chl *a* concentrations of ~ 2.8 $\mu\text{g/L}$ (Halbach et al., 2019) during late July and early August. The different Chl *a* concentrations observed between these studies does not directly follow differences in glacier grounding line and submarine discharge depths, as current models would predict (Hopwood et al., 2018; Oliver et al., 2020). That being said, model values are not directly comparable to single point in time Chl *a* measurements, so more work and samples are necessary to fully evaluate how measured Chl *a* compare to modeled productivity estimates. Meire et al. (2017), observed high (~ 20 $\mu\text{g/L}$) Chl *a* concentrations at glaciers with deeper grounding lines (≥ 140 m depth) than Sverdrup, lower turbidities (< 15 NTU), and a deeper euphotic zone than Sverdrup Glacier. However, the proximity of the closest Chl *a* measurement in that study was almost 10 km away from the glacier terminus, making direct comparisons to this work difficult. At Bowdoin glacier (in Greenland), however, Kanna et al., (2018) collected samples within 1 km of the terminus, finding similar proportions of glacial melt in the plume water at that

site (14%) as found here (13%). There, the highest observed Chl *a* (~6.5 µg/L) are similar to the maximum concentrations observed in this study (~7.5 µg/L). This is surprising, considering that Sverdrup has an estimated grounding line of >30 m depth compared to >200 m depth at Bowdoin Glacier. However, Kanna et al. (2018) did find elevated Chl *a* concentrations nearly 20 km into Bowdoin Fjord, while we see an elevated Chl *a* response extending a maximum of ~13.3 km from Sverdrup's terminus. The confined walls of Bowdoin fjord, different meltwater fluxes, and deeper grounding line may induce a larger degree of circulation, promoting similar levels of productivity farther away from the glacier terminus in the case of Bowdoin Glacier relative to Sverdrup Glacier. In Kongsfjorden (Svalbard), at both Kronebreen and Kongsvegen glaciers (discharge ~70 m depth) and Conwaybreen and Kongsbreen glaciers (discharge <10 m depth), Chl *a* concentrations were universally low (Halbach et al., 2019). In these cases, the marine waters around the deeper (~70 m depth) glaciers had lower Chl *a* concentrations (0.2–1.9 µg/L) likely due to higher turbidity, with differences in particle size and type (carbonate vs. silicates) between the sites playing an important role in light limitation. Thus, the “productivity continuum” between land terminating and tidewater glaciers, as defined by grounding line depth, does not appear to entirely hold for shallow tidewater glacier systems. Indeed, productivity at Sverdrup Glacier may be similar to or higher than productivity at other glaciers with deeper grounding lines (Halbach et al., 2019; Kanna et al., 2018). However, more study is clearly necessary to understand the full range of controls on entrainment, upwelling, nutrient delivery, and productivity at shallow tidewater glaciers.

5. Conclusions

Historically, tidewater glaciers have been identified as areas of heightened productivity (Lydersen et al., 2014; Vibe, 1939). Recently, glacially-induced upwelling of nutrient-rich deep

water has been proposed as a mechanism that can support primary productivity at the termini of tidewater glaciers in Alaska, Greenland, Svalbard, and Antarctica (Arimitsu et al., 2016; Lydersen et al., 2014; Meire et al., 2017). No study has been conducted on this topic in the CAA in almost 50 years (Apollonio, 1973). Here we find that carbon and nutrient concentrations in glacial melt are too low to enrich surface marine concentrations in the coastal ocean. However, similar to other studies, glacially-derived organic carbon exported within submarine discharge appears to be more bioavailable than marine carbon in the receiving seawater. We also observe that as the submarine discharge plume rises at the terminal ice cliff, it impacts the hydrography of the surrounding water column, inducing upwelling of intermediate (>30 m depth) marine water with elevated nutrient concentrations. The heightened Chl *a* concentrations observed at the interface between turbid freshened water and upwelled marine water close to the glacier terminus suggests that tidewater glaciers with shallow submarine outlets can promote primary productivity during nutrient-limited times of year.

Based on nutrient concentrations and Chl *a* response, Sverdrup Glacier falls between deep tidewater and land terminating glaciers, while it lies near the shallow end of the spectrum of grounding line depths (Hopwood et al., 2018). Compared to many glaciers examined in previous studies, Sverdrup Glacier is less dynamic, with a smaller meltwater flux and a shallower depth of submarine discharge. However, within 4 km of its terminus, the marine waters distal to Sverdrup Glacier is may be as productive as tidewater glaciers in Svalbard and Greenland with deeper grounding lines (Halbach et al., 2019; Kanna et al., 2018). The differences between deep and shallow tidewater glaciers in the magnitude and variability of observed nutrient and Chl *a* concentrations speak to the importance of determining the impacts of runoff on a variety of proglacial aquatic environments. Further, simultaneous measurements of carbon and

macronutrients in both on-ice and marine environments allowed us to detect glacially-induced entrainment of deep water and estuarine upwelling in Brae Bay, while confirming that glacial concentrations were too low to augment downstream nutrient and carbon pools. With continued retreat of large tidewater glaciers in Arctic seas, future work on how shallow tidewater glaciers affect downstream marine ecosystems will only become more relevant to the region as a whole.

Figure S2.2. Sverdrup surface mass balance validation.

(a) A map of Sverdrup Glacier showing the locations of weather stations (stars), mass balance stakes (green circles), with the catchment basin (RGI Consortium, 2017) outlined in black. (b) Plots comparing measured and modeled cumulative SMB at each weather station. The differences were used to calculate the bias between modeled RACMO2.3 and measured mass balance.

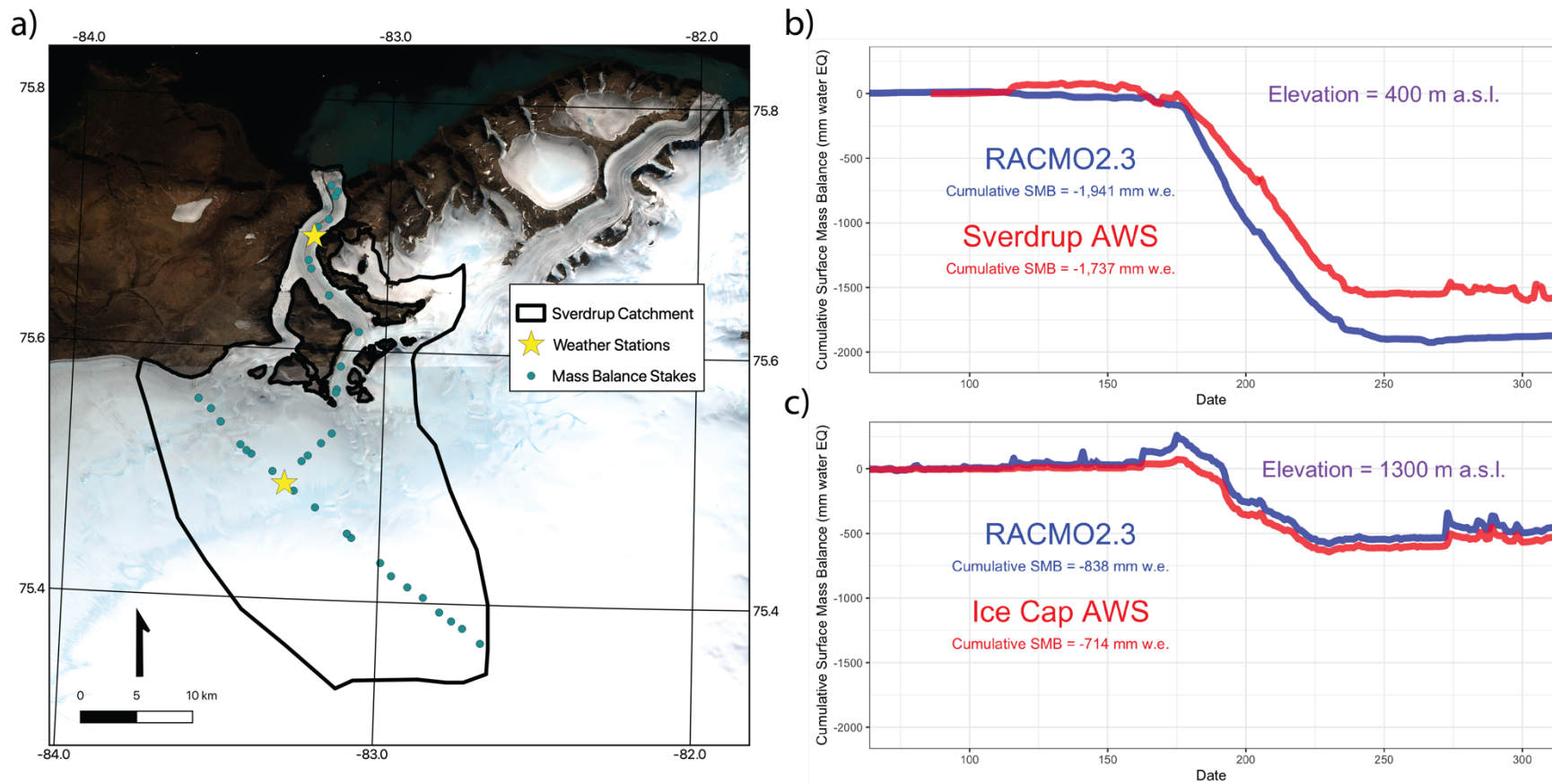


Figure S2.3. Time-lapse camera image summary.

(a) Time-lapse camera image of Brae Bay with Sverdrup Glacier and other landmasses removed to restrict color analysis to the ocean surface. The turbid submarine plume can be seen in the foreground. (b) The result of k-means colour-based pixel clustering (n=10) with plume pixels identified in red and non-plume pixels in blue. (c) Correlation between plume pixel count (corrected to relative area) and cumulative surface mass balance from the Sverdrup AWS.

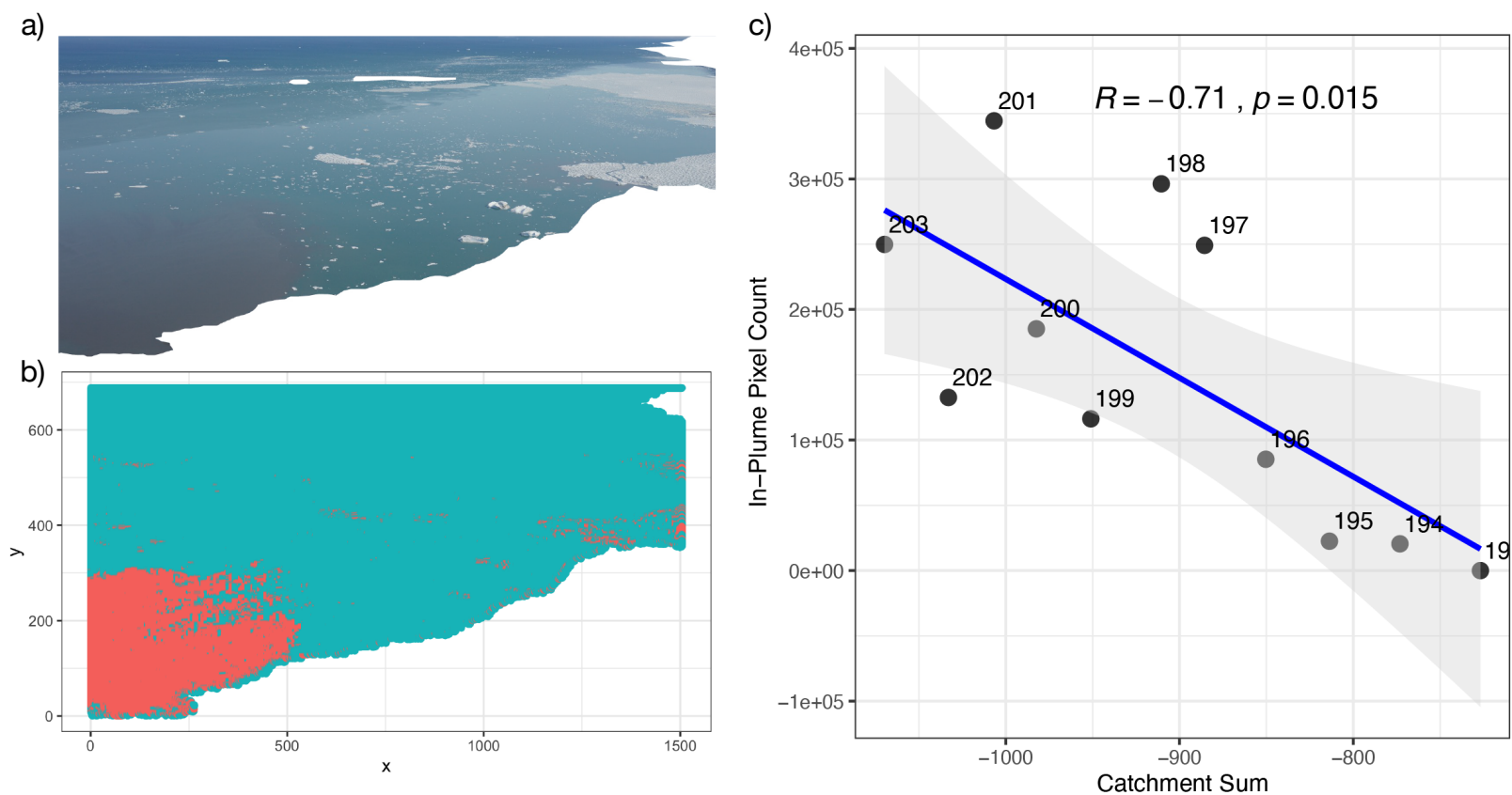


Figure S2.4. $\delta^{18}\text{O}$ versus salinity.

(a) $\delta^{18}\text{O}$ versus salinity in spring and summer glacial meltwater, marine plume water (>10% glacial melt using Equation 2b), and surface (0-10m), near surface (10-100m), and deep (>100m) marine water. Black diamonds denote Jones Sound deep water (JS), supraglacial meltwater (SM), marginal runoff (MR), sea-ice meltwater (SI), polar water (PW), and Baffin Bay deep water (BB) end-members (MR, SI, PW, BB, from Alkire, 2010). (b) An enlarged version of (a), highlighting marine samples.

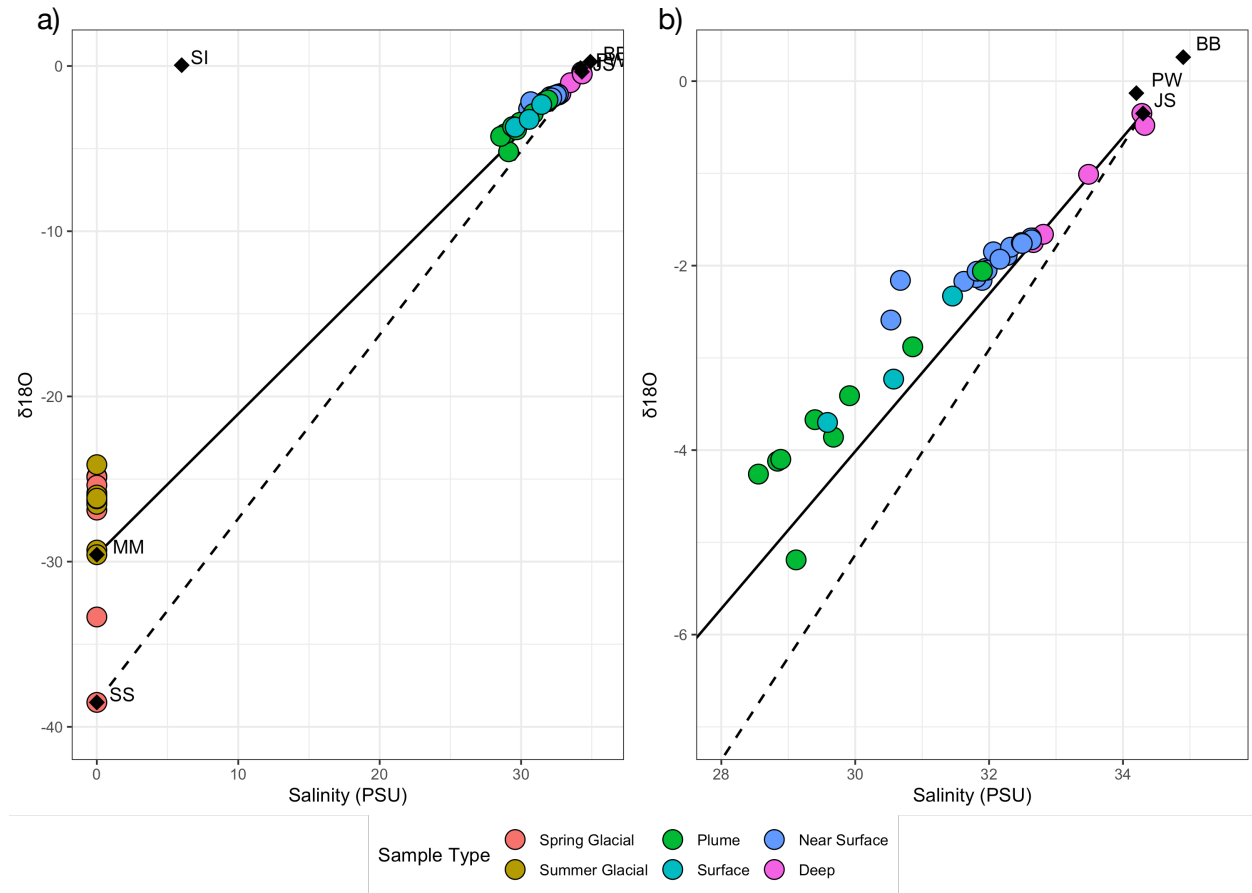


Figure S2.5. Box plots of marine nutrient ratios.

(a) and (b) plots denote different y-scales. Red dotted lines represent the Redfield ratio between the elements on the x-axis. Marine samples and some spring glacial samples are NO_3^- limited with respect to both P and Si. The whiskers extend to 1.5 times the inter-quartile range (distance between first and third quartile) in each direction.

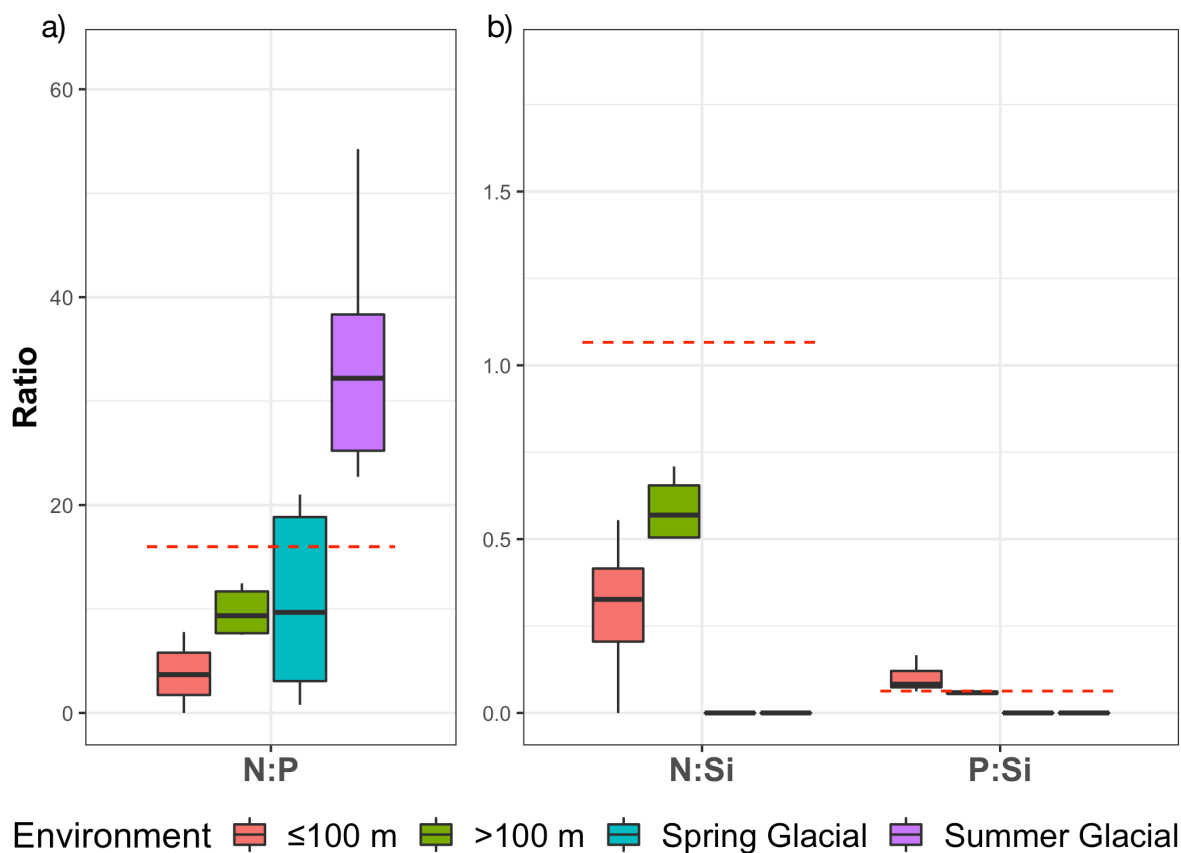


Table S2.1. Summary of samples collected and presented in this study.

Sample ID	Field Season	Water Type	Latitude	Longitude	Date Sampled
SVD-E-BI	Spring	Glacial	75.721883	-83.135511	4/23/2019
SVD-E-CI	Spring	Glacial	75.721883	-83.135511	4/23/2019
SVD-E-OW	Spring	Glacial	75.721883	-83.135511	4/24/2019
SVD-S-SI1	Spring	Glacial	75.690072	-83.24175	4/27/2019
SVD-S-SI2	Spring	Glacial	75.680422	-83.241139	5/7/2019
SVD-S-SS1	Spring	Glacial	75.690072	-83.24175	4/27/2019
SVD-S-SS2	Spring	Glacial	75.680422	-83.241139	5/7/2019
SVD-W-BI	Spring	Glacial	75.6932	-83.295547	4/27/2019
SVD-W-CI	Spring	Glacial	75.6932	-83.295547	4/27/2019
SVD-W-EI	Spring	Glacial	75.6932	-83.295547	4/27/2019
Ter_122	Summer	Glacial	75.45251	-83.9642	8/11/2019
Ter_123	Summer	Glacial	75.431782	-83.75203	8/10/2019
Ter_124	Summer	Glacial	75.324576	-83.61921	8/10/2019
Ter_125	Summer	Glacial	75.44951	-83.9624	8/10/2019
Ter_137	Summer	Glacial	75.324576	-83.61921	8/17/2019
Ter_138	Summer	Glacial	75.45251	-83.9642	8/10/2019
Ter_142	Summer	Glacial	75.44951	-83.96	8/11/201
Ter_144	Summer	Glacial	75.431782	-83.75203	8/11/2019
Ter_145	Summer	Glacial	75.4410.28	-82.425797	8/11/2019
Ter_150	Summer	Glacial	75.324576	-83.61921	8/11/2019
Ter_156	Summer	Glacial	75.45251	-83.9642	8/11/2019
VIO_22_2	Summer	Marine	75.745318	-83.286913	8/4/2019
VIO_22_3	Summer	Marine	75.745304	-83.286712	8/4/2019
VIO_22_4	Summer	Marine	75.744421	-83.283686	8/4/2019
VIO_23_2	Summer	Marine	75.749411	-83.195611	8/4/2019
VIO_23_3	Summer	Marine	75.749457	-83.194641	8/4/2019
VIO_24_2	Summer	Marine	75.750464	-83.194493	8/5/2019
VIO_24_3	Summer	Marine	75.750653	-83.192476	8/5/2019
VIO_25_2	Summer	Marine	75.76624	-83.114772	8/5/2019
VIO_25_3	Summer	Marine	75.765982	-83.113633	8/5/2019
VIO_26_2	Summer	Marine	75.766485	-83.160463	8/5/2019
VIO_26_3	Summer	Marine	75.766634	-83.159086	8/5/2019
VIO_27_2	Summer	Marine	75.766401	-83.223602	8/5/2019
VIO_27_3	Summer	Marine	75.766907	-83.222663	8/5/2019
VIO_27_4	Summer	Marine	75.767907	-83.22156	8/5/2019

VIO_28_2	Summer	Marine	75.763739	-83.28998	8/5/2019
VIO_28_3	Summer	Marine	75.76363	-83.290265	8/5/2019
VIO_29_2	Summer	Marine	75.749558	-83.201819	8/5/2019
VIO_29_3	Summer	Marine	75.749648	-83.202058	8/5/2019
VIO_30_10	Summer	Marine	75.762128	-83.242813	8/6/2019
VIO_30_4	Summer	Marine	75.759826	-83.236499	8/6/2019
VIO_30_5	Summer	Marine	75.759945	-83.234649	8/6/2019
VIO_30_9	Summer	Marine	75.761268	-83.243766	8/6/2019
VIO_31_2	Summer	Marine	75.827572	-82.979912	8/7/2019
VIO_31_3	Summer	Marine	75.827551	-82.979653	8/7/2019
VIO_31_4	Summer	Marine	75.82693	-82.976227	8/7/2019
VIO_31_5	Summer	Marine	75.826822	-82.976102	8/7/2019
VIO_32_2	Summer	Marine	75.891288	-82.918896	8/7/2019
VIO_32_3	Summer	Marine	75.892769	-82.9243	8/7/2019
VIO_32_7	Summer	Marine	75.891282	-82.923124	8/7/2019
VIO_32_8	Summer	Marine	75.892368	-82.926896	8/7/2019
VIO_33_2	Summer	Marine	75.938474	-82.795895	8/7/2019
VIO_33_3	Summer	Marine	75.938601	-82.796334	8/7/2019
VIO_33_4	Summer	Marine	75.932145	-82.769379	8/7/2019
VIO_33_5	Summer	Marine	75.935699	-82.780024	8/7/2019

Chapter 3: Conclusions

1. Research Conclusions

This thesis focuses on the role that glacial meltwater plays in downstream marine ecosystems by delivering nutrients and carbon to the ocean surface in the CAA. Herein, I established that the nutrient (NO_3^- , PO_4^{3-} , and SiO_4^{4-}) and DOC concentrations in summer glacial melt from Sverdrup are not high enough to augment downstream concentrations. However, the DOM exported from Sverdrup Glacier was significantly more protein-like, and potentially more bioavailable than marine carbon. We were able to detect a rising turbid and oxygen-rich meltwater plume which was released below the nutricline in Brae Bay (≥ 30 m depth), delivering nutrients to the surface within 4 km of the glacier terminus. Heightened Chl *a* concentrations were also observed in areas of upwelling close to Sverdrup Glacier. The delivery of nutrients occurs at a time when primary producers are nutrient limited, suggesting that melt from shallow tidewater glaciers, like Sverdrup Glacier, may impact primary productivity in downstream ecosystems.

2. Ongoing analyses

To provide a broader context for the impacts of glacial melt in the CAA, a larger analysis of tidewater glaciers in Jones Sound (Figure 1.2) has also been conducted. Similar marine stations were sampled at three other tidewater glaciers during the 2019 summer field season as well as at two non-glacierized sites. Of the four glaciers studied (Belcher, Jakeman, Sydkap, and Sverdrup) studied, Sverdrup Glacier had the second-smallest annual flux, and the shallowest discharge depth (Table 3.1). This work will be published separately, but results show that surface waters of glacierized regions contained significantly more macronutrients (nitrogen, silica, phosphorus) and

micronutrients (iron, manganese) than those of non-glacierized regions. The two glaciers with the deepest grounding lines (Belcher and Sydkap, Table 3.1) had the highest nitrate, phosphate, and silicate surface concentrations in the surface waters (Figure 3.1). Sverdrup and Jakeman glaciers both have grounding lines more than 100 m shallower than those of Belcher and Sydkap, but while Jakeman Glacier had nutrient concentrations comparable to those found at the non-glacierized sites, concentrations at Sverdrup Glacier were similar to those found at Belcher and Sydkap (Figure 3.1). This is likely explained by the fact that only a small proportion (25%) of Jakeman's calving front is in the water (Table 3.1), and thus, a significant amount of its discharge is released first onto land, rather than directly into the ocean. In addition to macronutrients, total dissolvable metal micronutrients (Fe, Mn) are high at Belcher, Sydkap, and Sverdrup while lower at Jakeman. Sverdrup Glacier had particularly high Fe and Mn concentrations (Figure 3.1), on par with the highest total dissolvable metal micronutrient concentrations observed in glacial systems (Bhatia et al., in preparation). This is not surprising in that samples from Sverdrup Glacier were collected from the discharge plume extensively, given that was the only site where the turbid plume was visible at the surface. Based on the results described in this thesis, glacially-induced upwelling of deep water is likely an important source of macronutrients to surface coastal waters distal to other tidewater glaciers in Jones Sound. Moreover, submarine discharge also appears to be a direct source of Fe and Mn to the surface ocean. Further work is still required to determine how important these glacially-derived macro- and micronutrients are to marine productivity in Jones Sound. However, it is surprising that the coastal waters surrounding Sverdrup Glacier, which has a grounding line nearly an order of magnitude shallower than the deepest glaciers draining into Jones Sound, had similar surface macronutrient concentrations to those found in front of deeper glacial systems, and very high metal micronutrient concentrations.

3. Limitations and future research

This study is limited in that it only provides a baseline characterization of melt from a single glacier over a single melt season. Further, while Chl *a* is a good proxy for primary productivity, neither primary nor secondary productivity were measured either in the marine environment or via incubations. Determining how glacially-mediated nutrient delivery directly affects productivity in Jones Sound is therefore not possible without further study. As the first study of glacial melt in Jones Sound in nearly half a century, there is a lack of spatial and temporal data to put these findings into a larger historical context. While existing studies in Greenland, Svalbard, and Alaska provide a general context for this work, the lack of similar CAA studies makes extrapolating these findings to other regions difficult.

To gain further understanding of how tidewater glaciers impact nutrient and carbon availability in downstream environments, this study would benefit from additional seasonal context. Data in this thesis focuses on only two time points (late spring and late summer) in a single year, and the lack of temporal continuity in measurements makes determining seasonal and annual variability challenging. There is also a deficiency in the spatial resolution of this study, with only 12 marine stations covering >50 km² of Brae Bay. Additional transects would allow for more accurate tracking of the subglacial plume and its impact on the marine environment. An analysis of mineral species entrained in both on-ice and marine waters would help to better identify the potential source of crustal nutrients (phosphate, silica, iron), while nitrogen isotope data could help identify the source of marine surface nutrients. Finally, more in-depth molecular analysis of the phytoplankton and microbial communities themselves would provide critical lacking insight into how marine biological communities at the base of the food web respond to and metabolize glacially-influenced carbon and nutrients. Additional work is clearly needed to gauge the impact

of melting glaciers on nutrient and carbon availability and marine productivity response in the CAA. Only with such additional study will it be possible to model the biogeochemical impact of CAA tidewater glaciers and how it may change in the future.

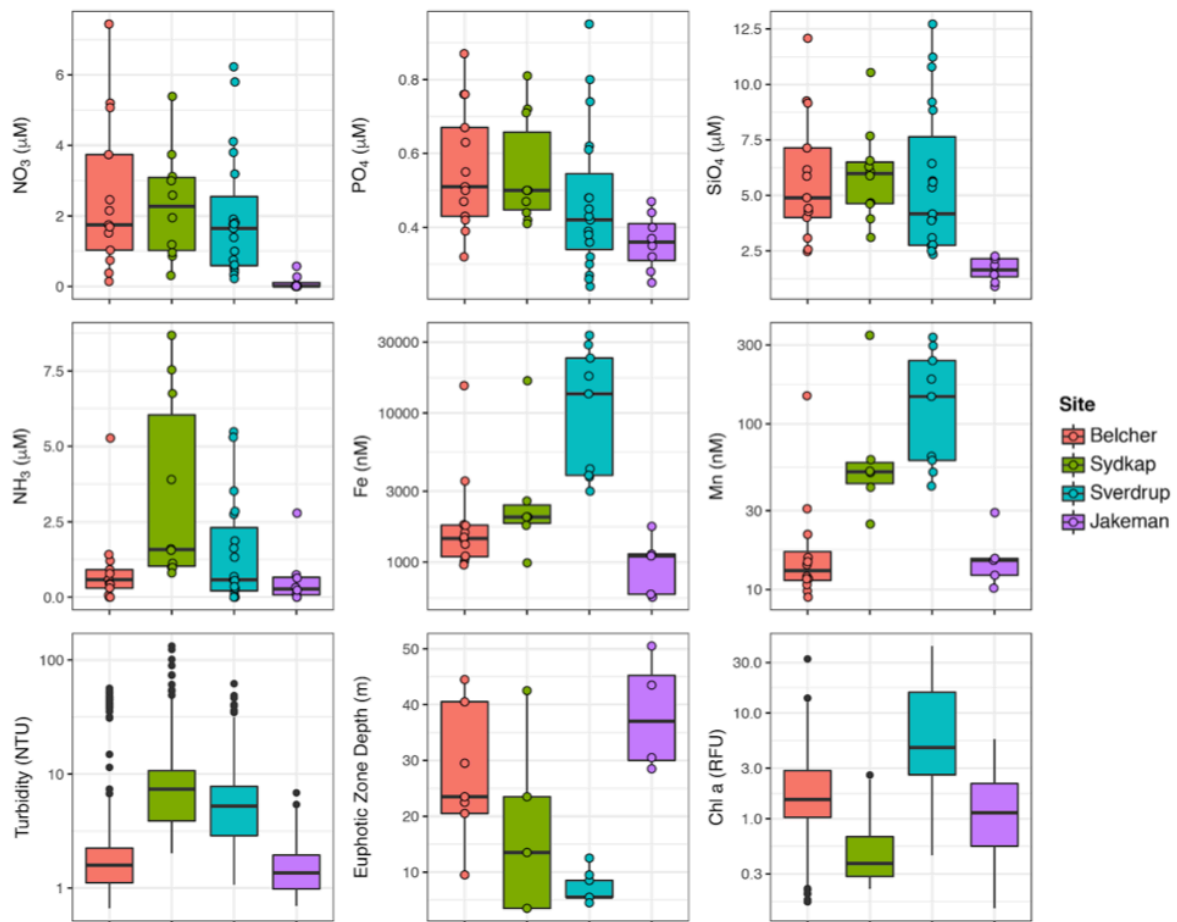
Table 3.1. Summary of characteristics of tidewater glaciers studied in the larger Jones Sound study.

Bias-corrected melt runoff values are reported for the 2019 summer melt season. Glacier basin areas are from the Randolph Glacier Inventory v6 (RGI Consortium, 2017). Errors for summer melt run-off, calving flux, elevation of the glacier bed at the terminus, and terminus retreat are indicated in brackets. Values in the last three columns (δ) were measured at the centerline only. Submarine discharge depth at Sverdrup glacier (*) is likely deeper than indicated by the elevation of the glacier bed down the terminus centerline. Values for annual calving flux were obtained from Van Wychen et. al. (2020). Ice thickness and elevation of glacier bed at the termini were obtained from NASA geophysical aerial surveys conducted in 2012 and 2014.

Glacier system	Location	Basin area (km ²)	Terminus width (km)	Width of marine terminating portion (km)	Summer melt (Gt/yr)	Calving flux (Gt/y)	Ice thickness at terminus (m) δ	Terminus bed elevation (m a.s.l.) δ	Terminus retreat: 1999-2020 (m) δ
Belcher	Devon Ice Cap, Devon Is.	1134	11.9	9.8	0.75 (0.14)	0.29 (0.031)	271	-239	1669
Sydkap	Sydkap Ice Field, Ellesmere Is.	491	3.09	3.09	0.13 (0.06)	0.042 (0.007)	190	-140	1928
Sverdrup	Devon Ice Cap, Devon Is.	805	5.12	5.12	0.34 (0.10)	0.006 (0.004)	25	-21*	217
Jakeman	Manson Ice Field, Ellesmere Is.	670	12.9	3.1	0.55 (0.08)	N/A	51	-36 (10)	450 (100)

Figure 3.1. Comparisons of surface ocean waters at tidewater glaciers in the CAA.

Comparisons of surface (upper 40 m) ocean waters at tidewater glaciers in the CAA within 10-km of the ice front. Sites are organized by grounding line depth. Individual data points (corresponding to water samples at discrete depths) are shown for the nutrients and metal concentrations. Euphotic zone depth was estimated at 0.1% of surface PAR at each station (individual data points). Note the log scale for Fe, Mn, Turbidity and Chl a. The black line indicates the median value, and the lower and upper hinges correspond to the first (25th) and third (75th) quartiles, respectively. The whiskers extend to 1.5 times the inter-quartile range (distance between first and third quartile) in each direction, with outlier data beyond the whiskers plotted individually.



Works Cited

1. Aciego, S. M., Stevenson, E. I., & Arendt, C. A. (2015). Climate versus geological controls on glacial meltwater micronutrient production in southern Greenland. *Earth and Planetary Science Letters*, *424*, 51-58. doi:10.1016/j.epsl.2015.05.017
2. Alkire, M. B. (2010). *Differentiating Freshwater Contributions and their Variability to the Surface and Halocline Layers of Arctic and Subarctic Seas* (K. Falkner Ed. Vol. PhD. Thesis). Oregon State University: Oregon State University.
3. Andersen, M. L., Larsen, T. B., Nettles, M., Elosegui, P., van As, D., Hamilton, G. S., . . . Dahl-Jensen, D. (2010). Spatial and temporal melt variability at Helheim Glacier, East Greenland, and its effect on ice dynamics. *Journal of Geophysical Research*, *115*(F4), 6886-6894. doi:10.1029/2010jf001760
4. Anderson, R. S., Molnar, P., & Kessler, M. A. (2006). Features of glacial valley profiles simply explained. *Journal of Geophysical Research*, *111*(F1). doi:<https://doi.org/10.1029/2005JF000344>
5. Apollonio, S. (1973). Glaciers and nutrients in arctic seas. *Science*, *180*(4085), 491-493. doi:10.1126/science.180.4085.491
6. Arar, E. J., & Collins, G. B. (1997). *Method 445.0 In Vitro Determination of Chlorophyll a and Pheophytin in Marine and Freshwater Algae by Fluorescence*. Retrieved from Washington, DC:
7. Arimitsu, M. L., Hobson, K. A., Webber, D. N., Piatt, J. F., Hood, E. W., & Fellman, J. B. (2018). Tracing biogeochemical subsidies from glacier runoff into Alaska's coastal marine food webs. *Glob Chang Biol*, *24*(1), 387-398. doi:10.1111/gcb.13875
8. Arimitsu, M. L., Piatt, J. F., & Mueter, F. (2016). Influence of glacier runoff on ecosystem structure in Gulf of Alaska fjords. *Marine Ecology Progress Series*, *560*, 19-40. doi:10.3354/meps11888
9. Arrigo, K. R., van Dijken, G. L., Castelao, R. M., Luo, H., Rennermalm, Å. K., Tedesco, M., . . . Yager, P. L. (2017). Melting glaciers stimulate large summer phytoplankton blooms in southwest Greenland waters. *Geophysical Research Letters*, *44*, 6278-6285. doi:10.1002/2017GL073583
10. Azam, F., & Malfatti, F. (2007). Microbial structuring of marine ecosystems. *Nat Rev Microbiol*, *5*(10), 782-791. doi:10.1038/nrmicro1747
11. Beaton, A. D., Wadham, J. L., Hawkings, J., Bagshaw, E. A., Lamarche-Gagnon, G., Mowlem, M. C., & Tranter, M. (2017). High-Resolution in Situ Measurement of Nitrate in Runoff from the Greenland Ice Sheet. *Environ Sci Technol*, *51*(21), 12518-12527. doi:10.1021/acs.est.7b03121
12. Bennett, M. R. (2011). Ice-Marginal Processes. In S. V.P., S. P., & H. U.K. (Eds.), *Encyclopedia of Snow, Ice and Glaciers* (Vol. Encyclopedia of Earth Sciences Series). Dordrecht: Springer.

13. Benson, B. B., & Krause, D. (1984). The concentration and isotopic fractionation of oxygen dissolved in freshwater and seawater in equilibrium with the atmosphere. *Limnology and Oceanography*, *29*(3), 620-632. doi:10.4319/lo.1984.29.3.0620
14. Bergeron, M., & Tremblay, J.-É. (2014). Shifts in biological productivity inferred from nutrient drawdown in the southern Beaufort Sea (2003-2011) and northern Baffin Bay (1997-2011), Canadian Arctic. *Geophysical Research Letters*, *41*(11), 3979-3987. doi:10.1002/2014gl059649
15. Bhatia, M. P., Das, S. B., Longnecker, K., Charette, M. A., & Kujawinski, E. B. (2010). Molecular characterization of dissolved organic matter associated with the Greenland ice sheet. *Geochimica et Cosmochimica Acta*, *74*, 3768-3784. doi:10.1016/j.gca.2010.03.035
16. Bhatia, M. P., Das, S. B., Xu, L., Charette, M. A., Wadham, J. L., & Kujawinski, E. B. (2013a). Organic carbon export from the Greenland ice sheet. *Geochimica et Cosmochimica Acta*, *109*, 329-344. doi:10.1016/j.gca.2013.02.006
17. Bhatia, M. P., Kujawinski, E. B., Das, S. B., Breier, C. F., Henderson, P. B., & Charette, M. A. (2013b). Greenland meltwater as a significant and potentially bioavailable source of iron to the ocean. *Nature Geoscience*, *6*, 274-278. doi:10.1038/ngeo1746
18. Błaszczuk, M., Jania, J. A., & Hagen, J. O. (2009). Tidewater glaciers of Svalbard: Recent changes and estimates of calving fluxes. *Polish Polar Research*, *30*(2), 85-102.
19. Boon, S., Burgess, D. O., Koerner, R. M., & Sharp, M. J. (2010). Forty-seven Years of Research on the Devon Island Ice Cap, Arctic Canada. *ARCTIC*, *63*(1), 13-29. doi:10.14430/arctic643
20. Boon, S., & Sharp, M. (2003). The role of hydrologically-driven ice fracture in drainage system evolution on an Arctic glacier. *Geophysical Research Letters*, *30*(18), 1916-1919. doi:10.1029/2003gl018034
21. Box, J. E., Colgan, W. T., Wouters, B., Burgess, D. O., O'Neel, S., Thomson, L. I., & Mernild, S. H. (2018). Global sea-level contribution from Arctic land ice: 1971–2017. *Environmental Research Letters*, *13*(12), 125012. doi:10.1088/1748-9326/aaf2ed
22. Boyd, E. S., Lange, R. K., Mitchell, A. C., Havig, J. R., Hamilton, T. L., Lafreniere, M. J., . . . Skidmore, M. (2011). Diversity, abundance, and potential activity of nitrifying and nitrate-reducing microbial assemblages in a subglacial ecosystem. *Appl Environ Microbiol*, *77*(14), 4778-4787. doi:10.1128/AEM.00376-11
23. Bro, R. (1997). PARAFAC. Tutorial and applications. *Chemometrics and Intelligent Laboratory Systems*, *38*(2), 149-171. doi:10.1016/s0169-7439(97)00032-4
24. Brown, G. H. (2002). Glacier meltwater hydrochemistry. *Applied Geochemistry*, *17*(7), 855-883. doi:10.1016/s0883-2927(01)00123-8
25. Burgess, D. O. (2018). Validation of the RACMO2.3 surface mass-balance model over northwest Devon Ice Cap, Nunavut. *Geological Survey of Canada, Open File 8382*, 1-19. doi:10.4095/308355

26. Bush, E., & Lemmen, D. S. (2019). *Canada's Changing Climate Report*. Ottawa, ON: Government of Canada.
27. Cape, M. R., Straneo, F., Beard, N., Bundy, R. M., & Charette, M. A. (2018). Nutrient release to oceans from buoyancy-driven upwelling at Greenland tidewater glaciers. *Nature Geoscience*, *12*(1), 34-39. doi:10.1038/s41561-018-0268-4
28. Carroll, D., Sutherland, D. A., Hudson, B., Moon, T., Catania, G. A., Shroyer, E. L., . . . van den Broeke, M. R. (2016). The impact of glacier geometry on meltwater plume structure and submarine melt in Greenland fjords. *Geophysical Research Letters*, *43*(18), 9739-9748. doi:10.1002/2016gl070170
29. Catania, G. A., Stearns, L. A., Sutherland, D. A., Fried, M. J., Bartholomaeus, T. C., Morlighem, M., . . . Nash, J. (2018). Geometric Controls on Tidewater Glacier Retreat in Central Western Greenland. *Journal of Geophysical Research: Earth Surface*, *123*(8), 2024-2038. doi:10.1029/2017jf004499
30. CHS Nautical Chart 7310, S. (Cartographer). (2011). Jones Sound Nautical Chart 7310
31. Chu, V. W., Smith, L. C., Rennermalm, A. K., Forster, R. R., & Box, J. E. (2012). Hydrologic controls on coastal suspended sediment plumes around the Greenland Ice Sheet. *The Cryosphere*, *6*(1), 1-19. doi:10.5194/tc-6-1-2012
32. Coble, P. G. (1996). Characterization of marine and terrestrial DOM in seawater using excitation-emission matrix spectroscopy. *Marine Chemistry*, *51*(4), 325-346. doi:10.1016/0304-4203(95)00062-3
33. Coble, P. G. (2007). Marine optical biogeochemistry: the chemistry of ocean color. *Chem Rev*, *107*(2), 402-418. doi:10.1021/cr050350+
34. Cohen, J., Screen, J. A., Furtado, J. C., Barlow, M., Whittleston, D., Coumou, D., . . . Jones, J. (2014). Recent Arctic amplification and extreme mid-latitude weather. *Nature Geoscience*, *7*(9), 627-637. doi:10.1038/ngeo2234
35. Cohen, J., Zhang, X., Francis, J., Jung, T., Kwok, R., Overland, J., . . . Yoon, J. (2019). Divergent consensus on Arctic amplification influence on midlatitude severe winter weather. *Nature Climate Change*, *10*(1), 20-29. doi:10.1038/s41558-019-0662-y
36. Conley, D. J., Kilham, S. S., & Theriot, E. (1989). Differences in silica content between marine and freshwater diatoms. *Limnology and Oceanography*, *34*(1), 205-212. doi:10.4319/lo.1989.34.1.0205
37. Consortium, R. (2017). *Randolph Glacier Inventory – A Dataset of Global Glacier Outlines* [Digital Media].
38. Cook, A. J., Copland, L., Noel, B. P. Y., Stokes, C. R., Bentley, M. J., Sharp, M. J., . . . van den Broeke, M. R. (2019). Atmospheric forcing of rapid marine-terminating glacier retreat in the Canadian Arctic Archipelago. *Sci Adv*, *5*(3), eaau8507. doi:10.1126/sciadv.aau8507
39. Cress, P., & Wyness, R. (1961). The Devon Island Expedition: Observations of glacial movements. *ARCTIC*, *14*, 257-259.

40. Cutter, G. A., & Bruland, K. W. (2012). Rapid and noncontaminating sampling system for trace elements in global ocean surveys. *Limnology and Oceanography: Methods*, *10*(6), 425-436. doi:10.4319/lom.2012.10.425
41. Das, S. B., Joughin, I., Behn, M. D., Howat, I. M., King, M. A., Lizarralde, D., & Bhatia, M. P. (2008). Fracture propagation to the base of the Greenland Ice Sheet during supraglacial lake drainage. *Science*, *320*(5877), 778-781. doi:10.1126/science.1153360
42. De Souza Sierra, M. M., Donard, O. F. X., Lamotte, M., Belin, C., & Ewald, M. (1994). Fluorescence spectroscopy of coastal and marine waters. *Marine Chemistry*, *47*(2), 127-144. doi:10.1016/0304-4203(94)90104-x
43. Dmitrenko, I., Kirillov, S., Tremblay, B., Gratton, Y., Barber, D., & Rysgaard, S. (2016). Upwelling of Atlantic Water along the Canadian Beaufort Sea Continental Slope: Favorable Atmospheric Conditions and Seasonal and Interannual Variations. *Journal of Climate*, *29*(12), 4509-4523. doi:10.1175/jcli-d-15-0804.1
44. Dowdeswell, J. A., Benham, T. J., Gorman, M. R., Burgess, D., & Sharp, M. J. (2004). Form and flow of the Devon Island Ice Cap, Canadian Arctic. *Journal of Geophysical Research: Earth Surface*, *109*, F02002. doi:10.1029/2003JF000095
45. Dubnick, A., Barker, J., Sharp, M., Wadham, J., Lis, G., Telling, J., . . . Jackson, M. (2017). Characterization of dissolved organic matter (DOM) from glacial environments using total fluorescence spectroscopy and parallel factor analysis. *Annals of Glaciology*, *51*(56), 111-122. doi:10.3189/172756411795931912
46. Dubnick, A., Sharp, M., Danielson, B., Saidi-Mehrabad, A., & Barker, J. (2020). Basal thermal regime affects the biogeochemistry of subglacial systems. *Biogeosciences*, *17*(4), 963-977. doi:10.5194/bg-17-963-2020
47. Etherington, L. L., Hooge, P. N., Hooge, E. R., & Hill, D. F. (2007). Oceanography of Glacier Bay, Alaska: Implications for biological patterns in a glacial fjord estuary. *Estuaries and Coasts*, *30*(6), 927-944. doi:10.1007/bf02841386
48. Everett, A., Kohler, J., Sundfjord, A., Kovacs, K. M., Torsvik, T., Pramanik, A., . . . Lydersen, C. (2018). Subglacial discharge plume behaviour revealed by CTD-instrumented ringed seals. *Sci Rep*, *8*(1), 13467. doi:10.1038/s41598-018-31875-8
49. Fegel, T., Boot, C. M., Broeckling, C. D., Baron, J. S., & Hall, E. K. (2019). Assessing the Chemistry and Bioavailability of Dissolved Organic Matter From Glaciers and Rock Glaciers. *Journal of Geophysical Research: Biogeosciences*, *124*(7), 1988-2004. doi:10.1029/2018jg004874
50. Fellman, J. B., Hood, E., Raymond, P. A., Hudson, J., Bozeman, M., & Arimitsu, M. (2015). Evidence for the assimilation of ancient glacier organic carbon in a proglacial stream food web. *Limnology and Oceanography*, *60*(4), 1118-1128. doi:10.1002/lno.10088
51. Fellman, J. B., Hood, E., & Spencer, R. G. M. (2010a). Fluorescence spectroscopy opens new windows into dissolved organic matter dynamics in freshwater ecosystems: A review. *Limnology and Oceanography*, *55*(6), 2452-2462. doi:10.4319/lo.2010.55.6.2452

52. Fellman, J. B., Spencer, R. G. M., Hernes, P. J., Edwards, R. T., D'Amore, D. V., & Hood, E. (2010b). The impact of glacier runoff on the biodegradability and biochemical composition of terrigenous dissolved organic matter in near-shore marine ecosystems. *Marine Chemistry*, 121(1-4), 112-122. doi:10.1016/j.marchem.2010.03.009
53. Flowers, G. E. (2015). Modelling water flow under glaciers and ice sheets. *Proceedings of the Royal Society A: Mathematical, Physical and Engineering Sciences*, 471, 20140907. doi:10.1098/rspa.2014.0907
54. Garcia, H. E., Locarnini, R. A., Boyer, T. P., Antonov, J. I., Mishonov, A. V., Baranova, O. K., . . . Johnson, D. R. (2013). *World Ocean Atlas 2013. Vol. 3: Dissolved Oxygen, Apparent Oxygen Utilization, and Oxygen Saturation* (A. Mishonov Ed. Vol. NOAA Atlas NESDIS).
55. Gardner, A. S., Moholdt, G., Wouters, B., Wolken, G. J., Burgess, D. O., Sharp, M. J., . . . Labine, C. (2011). Sharply increased mass loss from glaciers and ice caps in the Canadian Arctic Archipelago. *Nature*, 473, 357-360. doi:10.1038/nature10089
56. Gascon, G., Sharp, M., & Bush, A. (2017). Changes in melt season characteristics on Devon Ice Cap, Canada, and their association with the Arctic atmospheric circulation. *Annals of Glaciology*, 54(63), 101-110. doi:10.3189/2013AoG63A601
57. Gray, L. (2005). Evidence for subglacial water transport in the West Antarctic Ice Sheet through three-dimensional satellite radar interferometry. *Geophysical Research Letters*, 32, L03501. doi:10.1029/2004gl021387
58. Halbach, L., Vihtakari, M., Duarte, P., Everett, A., Granskog, M. A., Hop, H., . . . Assmy, P. (2019). Tidewater Glaciers and Bedrock Characteristics Control the Phytoplankton Growth Environment in a Fjord in the Arctic. *Frontiers in Marine Science*, 6, 254. doi:10.3389/fmars.2019.00254
59. Hartley, C. H., & Dunbar, M. J. (1938). On the hydrographic mechanism of the so-called brown zones associated with tidal glaciers. *Journal of Marine Research*, 1, 305.
60. Hawkings, J., Wadham, J., Tranter, M., Telling, J., Bagshaw, E., Beaton, A., . . . Nienow, P. (2016). The Greenland Ice Sheet as a hot spot of phosphorus weathering and export in the Arctic. *Global Biogeochemical Cycles*, 30, 191-210. doi:10.1002/2015GB005237
61. Hawkings, J. R., Wadham, J. L., Benning, L. G., Hendry, K. R., Tranter, M., Tedstone, A., . . . Raiswell, R. (2017). Ice sheets as a missing source of silica to the polar oceans. *Nature Communications*, 8, 14198. doi:10.1038/ncomms14198
62. Hawkings, J. R., Wadham, J. L., Tranter, M., Lawson, E., Sole, A., Cowton, T., . . . Telling, J. (2015). The effect of warming climate on nutrient and solute export from the Greenland Ice Sheet. *Geochemical Perspectives Letters*, 94-104. doi:10.7185/geochemlet.1510
63. Holmes, R. M., McClelland, J. W., Peterson, B. J., Tank, S. E., Bulygina, E., Eglinton, T. I., . . . Zimov, S. A. (2011). Seasonal and Annual Fluxes of Nutrients and Organic Matter

- from Large Rivers to the Arctic Ocean and Surrounding Seas. *Estuaries and Coasts*, 35(2), 369-382. doi:10.1007/s12237-011-9386-6
64. Hood, E., Fellman, J., Spencer, R. G. M., Hernes, P. J., Edwards, R., D'Amore, D., & Scott, D. (2009). Glaciers as a source of ancient and labile organic matter to the marine environment. *Nature*, 462, 1044-1047. doi:10.1038/nature08580
65. Hopwood, M. J., Carroll, D., Browning, T. J., Meire, L., Mortensen, J., Krisch, S., & Achterberg, E. P. (2018). Non-linear response of summertime marine productivity to increased meltwater discharge around Greenland. *Nature Communications*, 9, 3256. doi:10.1038/s41467-018-05488-8
66. Hopwood, M. J., Carroll, D., Dunse, T., Hodson, A., Holding, J. M., Iriarte, J. L., . . . Meire, L. (2020). Review Article: How does glacier discharge affect marine biogeochemistry and primary production in the Arctic? *The Cryosphere Discussions*. doi:10.5194/tc-2019-136
67. Hubbard, B. P., Sharp, M. J., Willis, I. C., Nielsen, M. K., & Smart, C. C. (1995). Borehole water-level variations and the structure of the subglacial hydrological system of Haut Glacier d'Arolla, Valais, Switzerland. *Journal of Glaciology*, 41(139), 572-583. doi:10.3189/s0022143000034894
68. Jackson, R. H., Shroyer, E. L., Nash, J. D., Sutherland, D. A., Carroll, D., Fried, M. J., . . . Stearns, L. A. (2017). Near-glacier surveying of a subglacial discharge plume: Implications for plume parameterizations. *Geophysical Research Letters*, 44(13), 6886-6894. doi:10.1002/2017gl073602
69. Juul-Pedersen, T., Arendt, K. E., Mortensen, J., Blicher, M. E., Sogaard, D. H., & Rysgaard, S. (2015). Seasonal and interannual phytoplankton production in a sub-Arctic tidewater outlet glacier fjord, SW Greenland. *Marine Ecology Progress Series*, 524, 27-38. doi:10.3354/meps11174
70. Kanna, N., Sugiyama, S., Ohashi, Y., Sakakibara, D., Fukamachi, Y., & Nomura, D. (2018). Upwelling of Macronutrients and Dissolved Inorganic Carbon by a Subglacial Freshwater Driven Plume in Bowdoin Fjord, Northwestern Greenland. *Journal of Geophysical Research: Biogeosciences*, 123, 1666-1682. doi:10.1029/2017JG004248
71. Keeler, C. M. (1964). Relationship between climate, ablation, and runoff on the Sverdrup Glacier 1963, Devon Island, NWT. *Montreal: Arctic Institute of North America, Research Paper 27*, 125.
72. Kessler, M. A., Anderson, R. S., & Briner, J. P. (2008). Fjord insertion into continental margins driven by topographic steering of ice. *Nature Geoscience*, 1(6), 365-369. doi:10.1038/ngeo201
73. Koerner, R. M. (1970). The Mass Balance of the Devon Island Ice Cap, Northwest Territories, Canada, 1961-66. *Journal of Glaciology*, 9(57), 325-336. doi:10.3189/s0022143000022863

74. Koerner, R. M., Apollonio, S., Cowie, J. W., Voegtli, K., Cress, P., Wyness, R., & Greenhouse, J. P. (1961). The Devon Island Expedition. *ARCTIC*, 14(4). doi:10.14430/arctic3683
75. Kumar, V., Tiwari, M., Nagoji, S., & Tripathi, S. (2016). Evidence of Anomalously Low $\delta^{13}C$ of Marine Organic Matter in an Arctic Fjord. *Sci Rep*, 6, 36192. doi:10.1038/srep36192
76. Larsen, C. (2010). *IceBridge UAF Lidar Profiler LIB Geolocated Surface Elevation Triplets, Version 1*.
77. Lydersen, C., Assmy, P., Falk-Petersen, S., Kohler, J., Kovacs, K. M., Reigstad, M., . . . Zajaczkowski, M. (2014). The importance of tidewater glaciers for marine mammals and seabirds in Svalbard, Norway. *Journal of Marine Systems*, 129, 452-471. doi:10.1016/j.jmarsys.2013.09.006
78. Mankoff, K. D., Straneo, F., Cenedese, C., Das, S. B., Richards, C. G., & Singh, H. (2016). Structure and dynamics of a subglacial discharge plume in a Greenlandic fjord. *Journal of Geophysical Research: Oceans*, 121(12), 8670-8688. doi:10.1002/2016jc011764
79. McDougal, T. J., & Barker, P. M. (2011). *Getting started with TEOS-10 and the Gibbs Seawater (GSW) Oceanographic Toolbox*: SCOR/IAPSO WG127.
80. Meire, L., Mortensen, J., Meire, P., Juul-Pedersen, T., Sejr, M. K., Rysgaard, S., . . . Meysman, F. J. R. (2017). Marine-terminating glaciers sustain high productivity in Greenland fjords. *Global Change Biology*, 23, 5344-5357. doi:10.1111/gcb.13801
81. Meire, L., Mortensen, J., Rysgaard, S., Bendtsen, J., Boone, W., Meire, P., & Meysman, F. J. R. (2016). Spring bloom dynamics in a subarctic fjord influenced by tidewater outlet glaciers (Godthåbsfjord, SW Greenland). *Journal of Geophysical Research: Biogeosciences*, 121(6), 1581-1592. doi:10.1002/2015jg003240
82. Meire, L., Søgaard, D. H., Mortensen, J., Meysman, F. J. R., Soetaert, K., Arendt, K. E., . . . Rysgaard, S. (2015). Glacial meltwater and primary production are drivers of strong CO₂ uptake in fjord and coastal waters adjacent to the Greenland Ice Sheet. *Biogeosciences*, 12(8), 2347-2363. doi:10.5194/bg-12-2347-2015
83. Melling, H., Agnew, T. A., Falkner, K. K., Greenberg, D. A., Lee, C. M., Münchow, A., . . . Woodgate, R. A. (2008). Fresh-Water Fluxes via Pacific and Arctic Outflows Across the Canadian Polar Shelf. In R. R. Dickson, J. Meincke, & P. Rhines (Eds.), *Arctic–Subarctic Ocean Fluxes: Defining the Role of the Northern Seas in Climate* (pp. 193-247). Dordrecht: Springer Netherlands.
84. Milner, A. M., Khamis, K., Battin, T. J., Brittain, J. E., Barrand, N. E., Fureder, L., . . . Brown, L. E. (2017). Glacier shrinkage driving global changes in downstream systems. *Proc Natl Acad Sci U S A*, 114(37), 9770-9778. doi:10.1073/pnas.1619807114
85. Morlighem, M., Williams, C. N., Rignot, E., An, L., Arndt, J. E., Bamber, J. L., . . . Zinglensen, K. B. (2017). BedMachine v3: Complete Bed Topography and Ocean

- Bathymetry Mapping of Greenland From Multibeam Echo Sounding Combined With Mass Conservation. *Geophys Res Lett*, 44(21), 11051-11061. doi:10.1002/2017GL074954
86. Murphy, K. R., Stedmon, C. A., Graeber, D., & Bro, R. (2013). Fluorescence spectroscopy and multi-way techniques. PARAFAC. *Analytical Methods*, 5(23). doi:10.1039/c3ay41160e
 87. Muschitiello, F., D'Andrea, W. J., Schmittner, A., Heaton, T. J., Balascio, N. L., deRoberts, N., . . . Dokken, T. M. (2019). Deep-water circulation changes lead North Atlantic climate during deglaciation. *Nat Commun*, 10(1), 1272. doi:10.1038/s41467-019-09237-3
 88. Musilova, M., Tranter, M., Wadham, J., Telling, J., Tedstone, A., & Anesio, Alexandre M. (2017). Microbially driven export of labile organic carbon from the Greenland ice sheet. *Nature Geoscience*, 10(5), 360-365. doi:10.1038/ngeo2920
 89. Nienow, P., Sharp, M., & Willis, I. (1998). Seasonal changes in the morphology of the subglacial drainage system, Haut Glacier d'Arolla, Switzerland. *Earth Surface Processes and Landforms*, 23(9), 825-843. doi:10.1002/(sici)1096-9837(199809)23:9<825::Aid-esp893>3.0.Co;2-2
 90. Noël, B., van de Berg, W. J., Lhermitte, S., Wouters, B., Schaffer, N., & van den Broeke, M. R. (2018). Six Decades of Glacial Mass Loss in the Canadian Arctic Archipelago. *Journal of Geophysical Research: Earth Surface*, 123(6), 1430-1449. doi:10.1029/2017jf004304
 91. Ohashi, Y., Iida, T., Sugiyama, S., & Aoki, S. (2016). Spatial and temporal variations in high turbidity surface water off the Thule region, northwestern Greenland. *Polar Science*, 10(3), 270-277. doi:10.1016/j.polar.2016.07.003
 92. Oliver, H., Castelao, R. M., Wang, C., & Yager, P. L. (2020). Meltwater-Enhanced Nutrient Export From Greenland's Glacial Fjords: A Sensitivity Analysis. *Journal of Geophysical Research: Oceans*, 125(7). doi:10.1029/2020jc016185
 93. Östlund, H. G., & Hut, G. (1984). Arctic Ocean water mass balance from isotope data. *Journal of Geophysical Research*, 89(C4). doi:10.1029/JC089iC04p06373
 94. Painter, S. C., Henson, S. A., Forryan, A., Steigenberger, S., Klar, J., Stinchcombe, M. C., . . . Moore, C. M. (2014). An assessment of the vertical diffusive flux of iron and other nutrients to the surface waters of the subpolar North Atlantic Ocean. *Biogeosciences*, 11(8), 2113-2130. doi:10.5194/bg-11-2113-2014
 95. Pautler, B. G., Woods, G. C., Dubnick, A., Simpson, A. J., Sharp, M. J., Fitzsimons, S. J., & Simpson, M. J. (2012). Molecular characterization of dissolved organic matter in glacial ice: coupling natural abundance ¹H NMR and fluorescence spectroscopy. *Environ Sci Technol*, 46(7), 3753-3761. doi:10.1021/es203942y
 96. Pomeroy, L. R. (1974). The Ocean's Food Web, A Changing Paradigm. *BioScience*, 24(9), 499-504. doi:10.2307/1296885

97. Randelhoff, A., Holding, J., Janout, M., Sejr, M. K., Babin, M., Tremblay, J.-É., & Alkire, M. B. (2020a). Pan-Arctic Ocean Primary Production Constrained by Turbulent Nitrate Fluxes. *Frontiers in Marine Science*, 7. doi:10.3389/fmars.2020.00150
98. Randelhoff, A., Lacour, L., Marec, C., Leymarie, E., Lagunas, J., Xing, X., . . . Babin, M. (2020b). Arctic mid-winter phytoplankton growth revealed by autonomous profilers. *Sci Adv*, 6(39), 1-9. doi:10.1126/sciadv.abc2678
99. Ravier, E., & Buoncristiani, J. (2018). Chapter 12: Glaciohydrogeology. In J. v. d. Meer & J. Menzies (Eds.), *Past Glacial Environments*: Elsevier.
100. Redfield, A. C., Ketchum, B. H., & Richards, F. A. (1963). The Influence of Organisms on the Composition of the Sea Water. In M. N. Hill (Ed.), *The composition of seawater: Comparative and descriptive oceanography. The sea: ideas and observations on progress in the study of the seas* (Vol. 2, pp. 26-77). New York: Interscience Publishers.
101. Richards, K., Sharp, M., Arnold, N., Gurnell, A., Clark, M., Tranter, M., . . . Lawson, W. (1996). An Integrated Approach to Modelling Hydrology and Water Quality in Glacierized Catchments. *Hydrological Processes*, 10(4), 479-508. doi:10.1002/(sici)1099-1085(199604)10:4<479::Aid-hyp406>3.0.Co;2-d
102. Sarmiento, J., & Gruber, N. (2006). *Ocean Biogeochemical Dynamics*. Princeton, NJ: Princeton University Press.
103. Segawa, T., Ishii, S., Ohte, N., Akiyoshi, A., Yamada, A., Maruyama, F., . . . Takeuchi, N. (2014). The nitrogen cycle in cryoconites: naturally occurring nitrification-denitrification granules on a glacier. *Environ Microbiol*, 16(10), 3250-3262. doi:10.1111/1462-2920.12543
104. Serreze, M. C., & Barry, R. G. (2011). Processes and impacts of Arctic amplification: A research synthesis. *Global and Planetary Change*, 77(1-2), 85-96. doi:10.1016/j.gloplacha.2011.03.004
105. Sharp, M. (2005). Subglacial Drainage. In M. G. Anderson (Ed.), *Encyclopedia of Hydrological Sciences* (Vol. 167, pp. Chapter 14): John Wiley & Sons.
106. Shepherd, A., Ivins, E., Rignot, E., Smith, B., Broeke, M. v. d., Velicogna, I., . . . Wuite, J. (2020). Mass balance of the Greenland Ice Sheet from 1992 to 2018. *Nature*, 579(7798), 233-239. doi:10.1038/s41586-019-1855-2
107. Smith, H. J., Dieser, M., McKnight, D. M., SanClements, M. D., & Foreman, C. M. (2018). Relationship between dissolved organic matter quality and microbial community composition across polar glacial environments. *FEMS Microbiol Ecol*, 94(7). doi:10.1093/femsec/fiy090
108. Smith, H. J., Foster, R. A., McKnight, D. M., Lisle, J. T., Littmann, S., Kuypers, M. M., & Foreman, C. M. (2017). Microbial formation of labile organic carbon in Antarctic glacial environments. *Nature Geoscience*, 10(5), 356-359. doi:10.1038/ngeo2925
109. Sorensen, H. L., Thamdrup, B., Jeppesen, E., Rysgaard, S., & Glud, R. N. (2017). Nutrient availability limits biological production in Arctic sea ice melt ponds. *Polar Biol*, 40(8), 1593-1606. doi:10.1007/s00300-017-2082-7

110. St-Onge, M. R., Van Gool, J. A. M., Garde, A. A., & Scott, D. J. (2009). Correlation of Archaean and Palaeoproterozoic units between northeastern Canada and western Greenland: constraining the pre-collisional upper plate accretionary history of the Trans-Hudson orogen. *Geological Society, London, Special Publications*, 318(1), 193-235. doi:10.1144/sp318.7
111. Stedmon, C. A., & Markager, S. (2005). Resolving the variability in dissolved organic matter fluorescence in a temperate estuary and its catchment using PARAFAC analysis. *Limnology and Oceanography*, 50(2), 686-697. doi:10.4319/lo.2005.50.2.0686
112. Stedmon, C. A., Markager, S., & Bro, R. (2003). Tracing dissolved organic matter in aquatic environments using a new approach to fluorescence spectroscopy. *Marine Chemistry*, 82(3-4), 239-254. doi:10.1016/s0304-4203(03)00072-0
113. Stedmon, C. A., Markager, S., Tranvik, L., Kronberg, L., Slätis, T., & Martinsen, W. (2007). Photochemical production of ammonium and transformation of dissolved organic matter in the Baltic Sea. *Marine Chemistry*, 104(3-4), 227-240. doi:10.1016/j.marchem.2006.11.005
114. Stocker, T., D. Qin, G-K, P., LV, A., SK, A., NL, B., . . . SP, X. (2014). *Technical Summary. In Climate Change 2013 – The Physical Science Basis: Working Group I Contribution to the Fifth Assessment Report of the Intergovernmental Panel on Climate Change*. Retrieved from
115. Straneo, F., & Cenedese, C. (2015). The Dynamics of Greenland's Glacial Fjords and Their Role in Climate. *Ann Rev Mar Sci*, 7, 89-112. doi:10.1146/annurev-marine-010213-135133
116. Telling, J., Stibal, M., Anesio, A. M., Tranter, M., Nias, I., Cook, J., . . . Hodson, A. (2012). Microbial nitrogen cycling on the Greenland Ice Sheet. *Biogeosciences*, 9(7), 2431-2442. doi:10.5194/bg-9-2431-2012
117. Timmermans, M. L., & Marshall, J. (2020). Understanding Arctic Ocean Circulation: A Review of Ocean Dynamics in a Changing Climate. *Journal of Geophysical Research: Oceans*, 125(4), e2018JC014378. doi:10.1029/2018jc014378
118. Tranter, M., Sharp, M. J., Lamb, H. R., Brown, G. H., Hubbard, B. P., & Willis, I. C. (2002). Geochemical weathering at the bed of Haut Glacier d'Arolla, Switzerland? a new model. *Hydrological Processes*, 16(5), 959-993. doi:10.1002/hyp.309
119. Tremblay, J.-É., Anderson, L. G., Matrai, P., Coupel, P., Bélanger, S., Michel, C., & Reigstad, M. (2015). Global and regional drivers of nutrient supply, primary production and CO₂ drawdown in the changing Arctic Ocean. *Progress in Oceanography*, 139, 171-196. doi:10.1016/j.pocean.2015.08.009
120. Tremblay, J.-É., & Gagnon, J. (2009). *The effects of irradiance and nutrient supply on the productivity of Arctic waters: a perspective on climate change*. Paper presented at the NATO Science for Peace and Security Series C: Environmental Security.
121. Van Wychen, W., Burgess, D. O., Gray, L., Copland, L., Sharp, M., Dowdeswell, J. A., & Benham, T. J. (2014). Glacier velocities and dynamic ice discharge from the Queen

- Elizabeth Islands, Nunavut, Canada. *Geophysical Research Letters*, 41(2), 484-490. doi:10.1002/2013gl058558
122. Van Wychen, W., Copland, L., & Burgess, D. (2020). Ice Masses of the Eastern Canadian Arctic Archipelago. In S. O. & C. N. (Eds.), *Landscapes and Landforms of Eastern Canada. World Geomorphological Landscapes*: Springer.
 123. Van Wychen, W., Copland, L., Burgess, D. O., Gray, L., Schaffer, N., & Fisher, T. (2015). Glacier velocities and dynamic discharge from the ice masses of Baffin Island and Bylot Island, Nunavut, Canada. *Canadian Journal of Earth Sciences*, 52(11), 980-989. doi:10.1139/cjes-2015-0087
 124. Vibe, C. (1939). Preliminary investigations on shallow water animal communities in the Upernavik- und Thule-districts (northwest Greenland). *Meddelelser om Gronland*, 124, 1-43.
 125. Vögtli, K. (1967). D.C. Resistivity Soundings on Devon Island, N.W.T., Canada. *Journal of Glaciology*, 6(47), 635-642. doi:10.3189/s0022143000019900
 126. Wadham, J. L., Hawkings, J., Telling, J., Chandler, D., Alcock, J., O'Donnell, E., . . . Nienow, P. (2016). Sources, cycling and export of nitrogen on the Greenland Ice Sheet. *Biogeosciences*, 13(22), 6339-6352. doi:10.5194/bg-13-6339-2016
 127. Walker, S. A., Amon, R. M. W., Stedmon, C., Duan, S., & Louchouart, P. (2009). The use of PARAFAC modeling to trace terrestrial dissolved organic matter and fingerprint water masses in coastal Canadian Arctic surface waters. *Journal of Geophysical Research*, 114, G00F06. doi:10.1029/2009jg000990
 128. Wang, L., Sharp, M. J., Rivard, B., Marshall, S., & Burgess, D. (2005). Melt season duration on Canadian Arctic ice caps, 2000-2004. *Geophysical Research Letters*, 32(19), n/a-n/a. doi:10.1029/2005gl023962
 129. Wendisch, M., Brückner, M., Burrows, J., Crewell, S., Dethloff, K., Ebell, K., . . . Tegen, I. (2017). Understanding Causes and Effects of Rapid Warming in the Arctic. *Eos*, 98. doi:10.1029/2017eo064803
 130. Whalen, J. B., Wodicka, N., Taylor, B. E., & Jackson, G. D. (2010). Cumberland batholith, Trans-Hudson Orogen, Canada: Petrogenesis and implications for Paleoproterozoic crustal and orogenic processes. *Lithos*, 117(1-4), 99-118. doi:10.1016/j.lithos.2010.02.008
 131. Wolff, E. W. (2013). Ice sheets and nitrogen. *Philos Trans R Soc Lond B Biol Sci*, 368(1621), 20130127. doi:10.1098/rstb.2013.0127
 132. Woodgate, R. A., Aagaard, K., Swift, J. H., Falkner, K. K., & Smethie, W. M. (2005). Pacific ventilation of the Arctic Ocean's lower halocline by upwelling and diapycnal mixing over the continental margin. *Geophysical Research Letters*, 32(18), L18609. doi:10.1029/2005gl023999
 133. World Glacier Monitoring, S. (2008) Global glacier changes. In *Supplement to: World Glacier Monitoring Service (2008): Fluctuations of Glaciers 2000-2005*. Haeberli, W;

- Zemp, M; Paul, F; Hoelzle, M (eds.), ICSU (FAGS) / IUGG (IACS) / UNEP / UNESCO / WMO, World Glacier Monitoring Service, Zurich, Switzerland, IX, 266 pp, hdl:10013/epic.39784.d001: PANGAEA.
134. Wyatt, F. R., & Sharp, M. J. (2017). Linking surface hydrology to flow regimes and patterns of velocity variability on Devon Ice Cap, Nunavut. *Journal of Glaciology*, 61(226), 387-399. doi:10.3189/2015JoG14J109
135. Yamashita, Y., Fichot, C. G., Shen, Y., Jaffé, R., & Benner, R. (2015). Linkages among fluorescent dissolved organic matter, dissolved amino acids and lignin-derived phenols in a river-influenced ocean margin. *Frontiers in Marine Science*, 2(92). doi:10.3389/fmars.2015.00092
136. Zhang, Y., Chen, C., Beardsley, R. C., Gao, G., Lai, Z., Curry, B., . . . Xu, Q. (2016). Studies of the Canadian Arctic Archipelago water transport and its relationship to basin-local forcings: Results from AO-FVCOM. *Journal of Geophysical Research: Oceans*, 121(6), 4392-4415. doi:10.1002/2016jc011634
137. Zhu, Y., Suggett, D. J., Liu, C., He, J., Lin, L., Le, F., . . . Hao, Q. (2019). Primary Productivity Dynamics in the Summer Arctic Ocean Confirms Broad Regulation of the Electron Requirement for Carbon Fixation by Light-Phytoplankton Community Interaction. *Frontiers in Marine Science*, 6, 275. doi:10.3389/fmars.2019.00275